The Vaasa Migmatitic Complex (Svecofennian Orogen, Finland): Buildup of a LP-HT Dome During Nuna Assembly

Francis Chopin, Annakaisa Korja, Kaisa Nikkilä, Pentti Hölttä, Toivo Korja, Mohamed Abdel Zaher, Matti Kurhila, Olav Eklund, O. Tapani Rämö

Tectonics

RESEARCH ARTICLE
10.1029/2019TC005583

Key Points:
- Geophysical maps, deep seismic and magnetotelluric profiles and geological data are used to reveal the formation of an accretionary system
- The accretion of supracrustal rocks is responsible for the development of HT-LP metamorphism and channel flow of partially molten rocks
- The formation of an orocline terminates by the vertical mass redistribution of a migmatitic core in the hinge zone

Supporting Information:
- Supporting Information S1

Correspondence to:
F. Chopin,
chop1fran6@gmail.com;
f.chopin@unistra.fr

Citation:
Chopin, F., Korja, A., Nikkilä, K., Hölttä, P., Korja, T., Abdel Zaher, M., et al. (2020). The Vaasa migmatitic complex (Svecofennian orogen, Finland): Buildup of a LP-HT dome during Nuna assembly. *Tectonics*, *39*, e2019TC005583. https://doi.org/10.1029/2019TC005583

Received 20 MAR 2019
Accepted 11 OCT 2019
Accepted article online 24 JAN 2000

The Vaasa Migmatitic Complex (Svecofennian Orogen, Finland): Buildup of a LP-HT Dome During Nuna Assembly

Francis Chopin[1,2,3], Annakaisa Korja[1], Kaisa Nikkilä[1,4], Pentti Hölttä[5], Toivo Korja[6,7], Mohamed Abdel Zaher[6,8], Matti Kurhila[1,5], Olav Eklund[4], and O. Tapani Rämö[1]

[1]Department of Geosciences and Geography, University of Helsinki, Helsinki, Finland, [2]Université de Strasbourg, CNRS, IPGS UMR 7516, Strasbourg, France, [3]Center for Lithospheric Research, Czech Geological Survey, Prague, Czech Republic, [4]Geology and Mineralogy, Åbo Akademi University, Turku, Finland, [5]Geological Survey of Finland, Espoo, Finland, [6]Faculty of Technology, Oulu Mining School, Applied Geophysics, University of Oulu, Oulu, Finland, [7]Now at Exploration Geophysics, Geosciences and Environmental Engineering, Luleå University of Technology, Luleå, Sweden, [8]Now at Geomagnetic and Geoelectric Department, National Research Institute of Astronomy and Geophysics, Helwan, Egypt

Abstract Tectonic evolution of the Paleoproterozoic Vaasa migmatitic complex (VMC) in the central part of the Svecofennian accretionary orogen is deciphered using aeromagnetic and gravity maps, deep seismic and magnetotelluric profiles, and structural and metamorphic data. The VMC is a semicircular structure with migmatitic rim and granitic core composed of several subdomes. It evolved in three main tectonic events (D1–D3). The D1 event (ca. 1.89–1.88 Ga) corresponds to the stacking of supracrustal rocks and the formation of an inverted metamorphic gradient. Anatexis at LP-HT metamorphic conditions enabled the material to flow. The D2 event (ca. 1.88–1.87 Ga) corresponds to large-scale folding of the partially molten crust within an orocline. It is marked by folds with an E-W vertical axial planar foliation. The late D3 event resulted from mass redistribution owing to mechanical instabilities within the hinge of the orocline. It is marked by vertical shearing (ca. 1.87–1.85 Ga) in the marginal parts of the complex and along the granitoid subdomes. The seismic reflection profile (FIRE 3a) and magnetotelluric profiles (MT-PE and MT-B2) image large-scale D1 stacking structures within an accretionary prism. Near vertical breaks in crustal-scale reflectivity and conductivity models are interpreted as D3 shear zones. The VMC is an example of early mass and heat transfer within a collage of hot supracrustal rocks in an accretionary belt. Partial melting enhanced the flow of material, the production, and rise of magma as well as exhumation, marked by magmatic domes in the hinge of the orocline.

1. Introduction

The Paleoproterozoic Svecofennian orogen (1.9–1.8 Ga) has been intensively studied by a wide range of geological and geophysical methods. Most authors agree that it is an accretionary orogen and that it has been built from terranes and intervening sedimentary basins along an active continental margin (Figure 1a; Gaál & Gorbatschev, 1987; Gorbatschev & Bogdanova, 1993; Korja et al., 2006; Lahtinen et al., 2005; Nironen, 2017; Ward, 1987) of the Comlumbia/Nuna supercontinent (Meert, 2012; Rogers & Santosh, 2002; Zhao et al., 2002, 2004). The geodynamic and tectonic models driving the accretionary process are, however, under debate. Hermansson et al. (2008) suggested advancing and retreating subduction zones; Nikkilä et al. (2015) suggested accretion followed by collapse; Cagnard et al. (2007) suggested distributed thickening and lateral flow; and Lahtinen et al. (2014) proposed a model where the linear accretionary system is later buckled forming coupled oroclines (Lahtinen et al., 2017). Based on surface structural observations, Cagnard et al. (2006, 2007) suggested that Southern Finland Subprovince of the Svecofennian orogeny (Figure 1) has suffered from horizontal shortening, lateral and vertical mass and heat transfers resulting in the formation of pop-down structures, and exhumation of partially molten deep rocks (Chardon et al., 2009; Gapais et al., 2014). According to Cagnard et al. (2006, 2007), the orogenic fabric is characterized by subvertical orogenic structures affecting middle and upper orogenic levels and by granitoids. This structural pattern is broadly similar to that reported from other accretionary systems such as the Paleoproterozoic Mazatzal and Yavapay orogens in North America (Karlstrom & Williams, 1998), the Paleozoic Lachlan

10.1029/2019TC005583

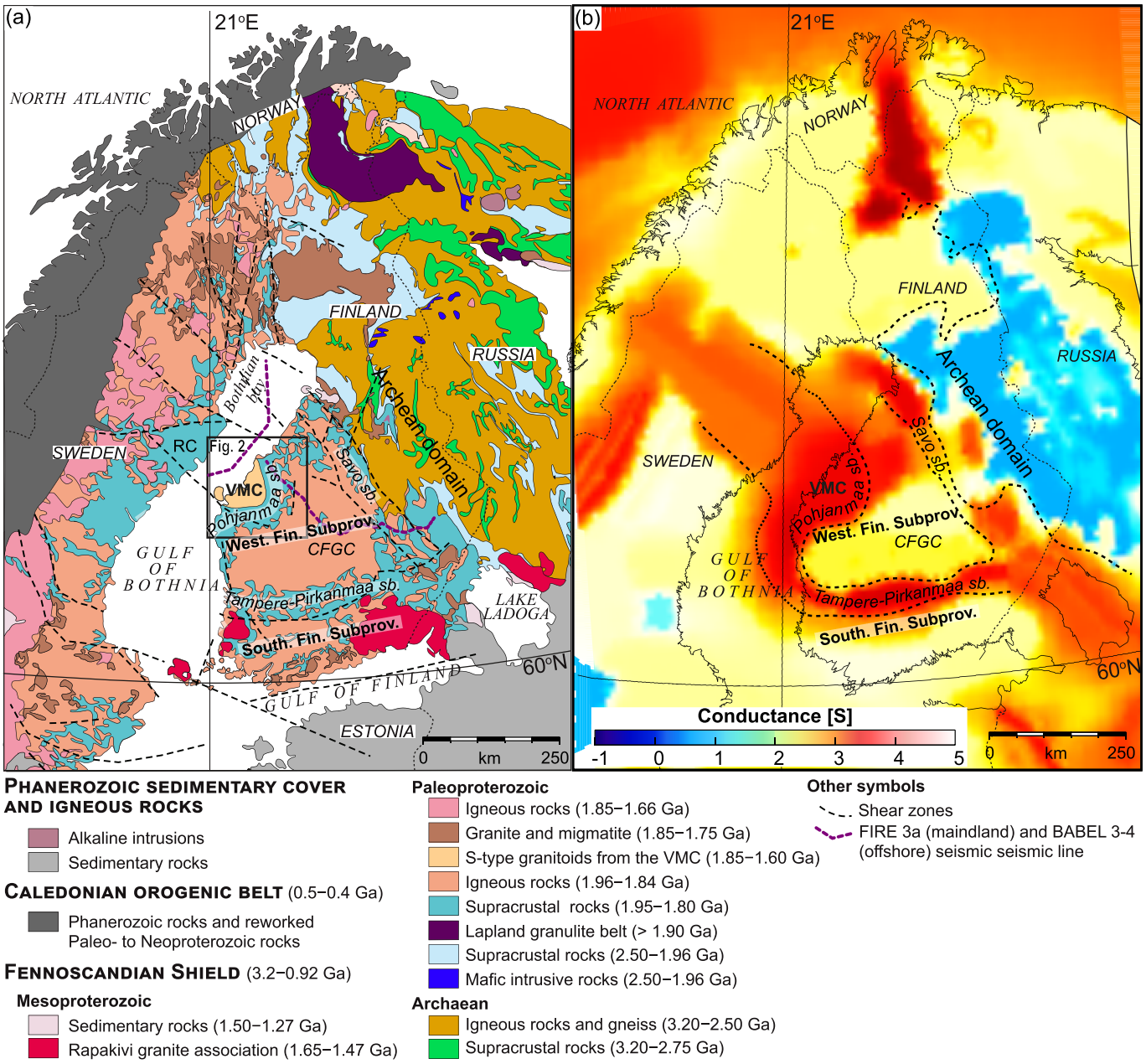

Figure 1. Main lithological and crustal conductivity features of Fennoscandian Shield. (a) A map of major tectonic units simplified after Koistinen et al. (2001). The study area is outlined with a black box (Figures 2 and 3). (b) A crustal conductance model after Korja et al. (2002). Crustal conductance (Siemens [S]) is estimated from published conductivity models from surface to the depth of 60 km (S = integral of thickness [m] multiplied by electrical conductivity [S/m]). Note that data from this paper (Figure 4; MT-PE and MT-B2 profiles) are not included in the model. CFGC = Central Finland Granitoid Complex; RC = Robertsfors complex; sb. = schist belt; VMC = Vaasa Migmatitic Complex.

orogen in Australia (Foster & Gray, 2000), or the Central Asian Orogenic Belt (CAOB) in China (Jiang et al., 2015). Crustal-scale geophysical profiles across the Svecofennian orogen (e.g., Korja & Heikkinen, 2005; Korja & Hjelt, 1993; Kukkonen et al., 2006; Lahtinen et al., 2009; Sorjonen-Ward, 2006), however, image moderate to shallow dipping structures at depth suggesting gently dipping rather than subvertical structures. The gently dipping structures have been interpreted either as thrust and stacking surfaces (e.g., Korja et al., 1993; Korja & Hjelt, 1993; Lahtinen et al., 2009; Sorjonen-Ward, 2006) or as extensional detachments (Korja et al., 2009; Torvela et al., 2013). Similar shallow dipping structures are found in the Lachlan orogen, where reflections are rooted at midcrustal level above a seismically transparent lower crust (Glen et al., 2002) or in

the Mongolian CAOB, where a clear geophysical discontinuity is found between orogenic upper and lower crusts (Guy et al., 2014).

Several tectonic models may explain the apparent discrepancy between the geological and geophysical observations. In the first model, the deep crustal horizontal fabrics reflect a younger horizontal channel flow (Beaumont et al., 2006; Vanderhaeghe & Teyssier, 2001) beneath the inherited steep fabric of a suprastructure as proposed, for instance, by Costa and Rey (1995), Culshaw et al. (2006), or Guy et al. (2015) for the French Massif Central, Grenville orogeny in Canada, or CAOB, respectively. In the second model, the upper-middle crust is deformed and folded above a rigid lower crustal and horizontal granulitic substratum as proposed, for example, by Lehmann et al. (2017). In the latter model, the deep horizontal and shallow vertical crustal structures are interpreted to reflect tectonic switching: HT extensional deformation associated with subduction rollback in the upper plate, followed by inversion and upright folding related to advancing subduction mode (Collins, 2002a, 2002b).

Torvela et al. (2013) proposed another alternative tectonic model for the Svecofennian orogeny. They interpret the deep crustal seismic reflections as a proxy for crustal-scale S-C structure (Berthé et al., 1979) of extensional shear bands (Kidan & Cosgrove, 1996). This would imply that the main orogenic fabric and the shear discontinuities are coeval and resulted from generalized horizontal spreading typical for late orogenic extensional collapse (Cosgrove, 1997; Dewey, 1988).

Exhumed accretionary systems, where upper and middle crustal blocks found next to each other, are ideal natural laboratories to study the relationships between upper and lower crustal deformation processes and thus intriguing incoherency between surface geological observations and deep crustal geophysical imagery.

The contrasting views on nature of crustal-scale deformation in accretionary systems in general and of Svecofennian orogeny in particular led us to undertake multidisciplinary investigations of the Vaasa migmatitic complex (VMC) located in the central part of this orogen. The VMC is located in a well-studied area with existing lithological, metamorphic, aeromagnetic, conductivity, and Bouguer anomaly data as well as transecting deep seismic reflection profiles (Figures 1–4). By combing legacy data with newly acquired detailed structural and metamorphic data (Figures 5–9) as well as magnetotelluric profiled data (Figures 4c and 4d), we aim to more precisely assess the structural, metamorphic, and tectonic evolution of study area. The newly structural observations will be compared to existing and new petrographic data in order to better constrain the deformation-metamorphism relationship. We will also investigate the deep crustal structure by combining the deep seismic reflection data with newly acquired magnetotelluric conductivity profiles. This approach allows us to propose a conceptual geodynamic model for the Svecofennian orogeny (Figure 11) and open new doors to globally reevaluate the deep crustal structures of accretionary systems.

2. Geological and Geophysical Setting

2.1. Svecofennian Accretionary Orogen

The 1.92–1.77 Gyr old Svecofennian orogen (Gaál & Gorbatschev, 1987; Gorbatschev & Bogdanova, 1993) formed in a long-lived accretionary system along the Paleoproterozoic Columbia/Nuna supercontinent margin (Zhao et al., 2002, 2004). It was a collage of island arcs and microcontinents (Bothnian, Keitele, and Bergslagen) and intervening basins (e.g., Bogdanova et al., 2015; Korja et al., 2006; Korja & Heikkinen, 2005; Lahtinen et al., 2005; Lahtinen et al., 2009; Nironen, 1997; Nironen, 2017). The accretion was associated with LP-HT regional metamorphism that reached anatexis (700–800 °C and 4–5 kbar; Korsman et al., 1997). Luukas et al. (2017) divided the Finnish part of the Svecofennian orogen into the Southern and Western Finland Subprovinces (Figure 1a); the latter being divided into the Central Finland Granitoid Complex (CFGC) and the Savo, Tampere-Pirkanmaa, and Pohjanmaa schist belts (Nironen et al., 2002). The CFGC, interpreted as a typical root zone of a magmatic arc (Rämö et al., 2001), comprises mainly (I-type) calc-alkalic to alkali-calcic granitoids (1.89–1.87 Ga; Nironen et al., 2000, Nikkilä et al., 2016) with minor amounts of mafic plutonic rocks and comagmatic volcanic sequences (Kähkönen, 2005; Korsman et al., 1997; Lahtinen et al., 2017; Nironen et al., 2000). It is surrounded by schist belts (Savo, Tampere-Pirkanmaa, and Pohjanmaa schist belts) made of supracrustal (meta)sediments (greywackes and pelites) and volcanic rocks. The age of the basin is about 1.92–1.90 Ga (Lahtinen et al., 2002, 2017), and its main

10.1029/2019TC005583

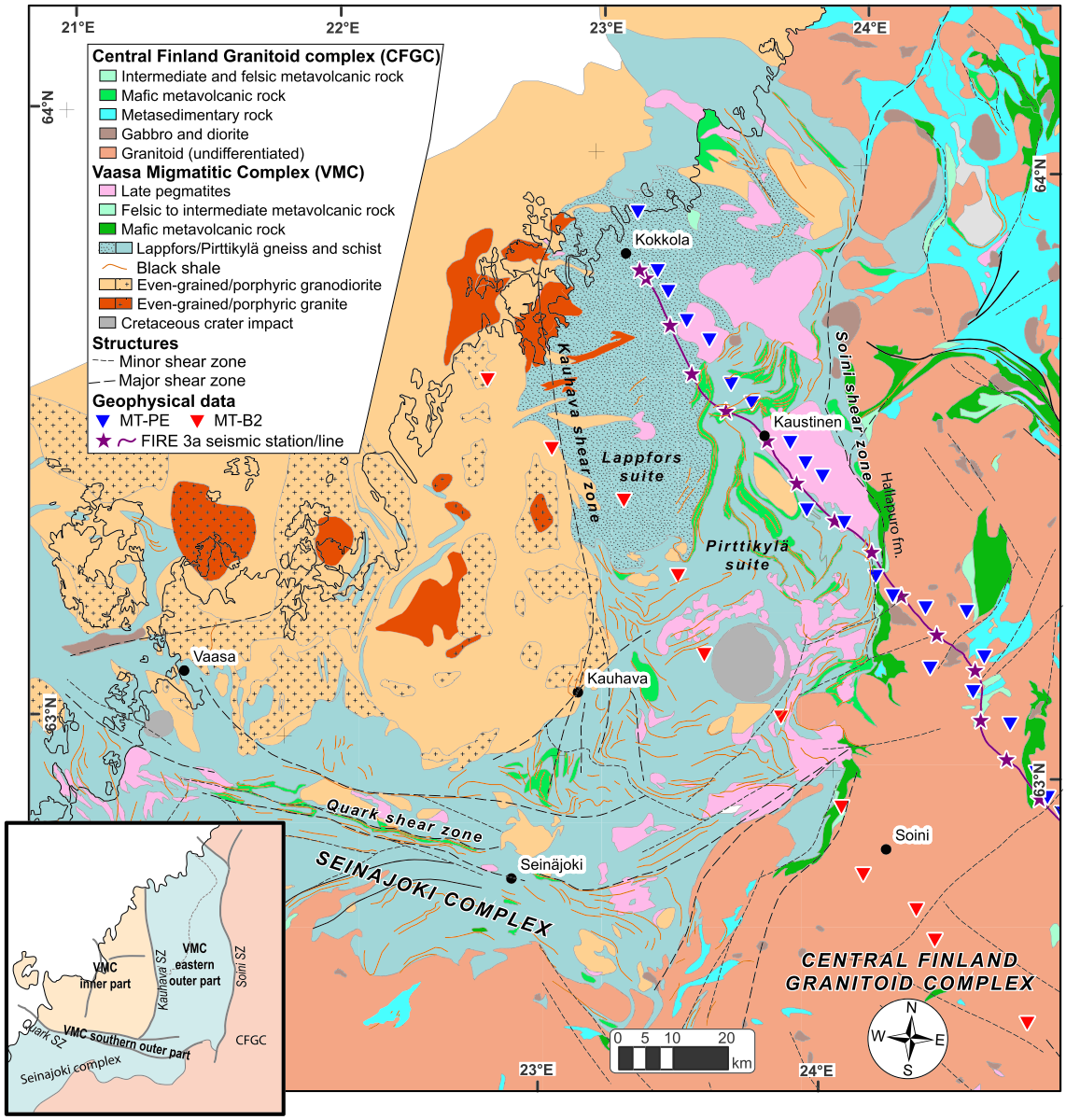

Figure 2. A lithological and structural map of the Vaasa migmatitic complex, modified after Korsman et al. (1997) and the digital bedrock map 1:200,000 and 1:1,000,000 from the Geological Survey of Finland (2012, 2017, respectively). CFGC = Central Finland granitoid complex; VMC = Vaasa migmatitic complex.

sedimentary source is the nearby Archean craton, with only few arc-derived sediments (Claesson et al., 1993; Kotilainen et al., 2016b; Lahtinen et al., 2002; Lahtinen et al., 2017).

The Svecofennian orogen is characterized by thick (52–65 km) three-layer crust and long, elongated crustal-scale conductors surrounding large resistive units (Figure 1b; Grad et al., 2009; Korja et al., 1993, 2002). High conductance anomalies (10,000–20,000 S) are interpreted to result from the presence of graphite- and sulfide-bearing black schists. In the central parts of the orogen, there is a large ellipsoidal granitoid batholith (150 by 120 km) surrounded by HT-LP metapelitic and metagreywacke units—the Vaasa migmatitic complex (VMC)—and underlain by one of the strongest and largest conductivity anomalies in the world (Figure 1b; Korja et al., 2002, 2013). The VMC is covered by low altitude airborne magnetic, electromagnetic (Korhonen, Aaro, All, Nevanlinna, et al., 2002,Korhonen, Aaro, All, Elo, et al., 2002; Leväniemi et al., 2009), and Bouguer anomaly data (Korhonen, Aaro, All, Nevanlinna, et al., 2002,Korhonen, Aaro, All, Elo, et al., 2002). In addition, the area is covered by deep seismic reflection (FIRE3 onshore and BABEL3&4 offshore)

10.1029/2019TC005583

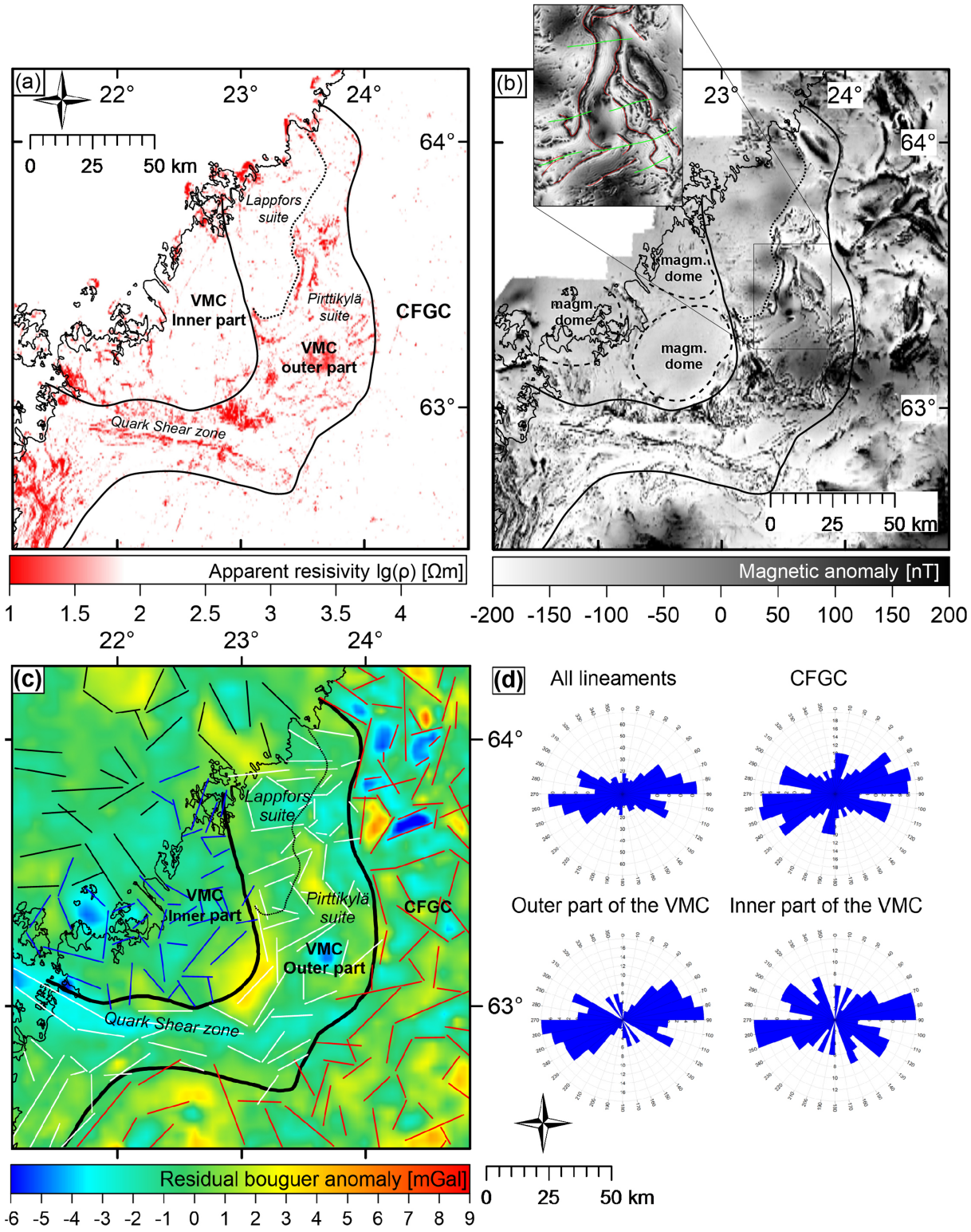

Figure 3. Geophysical maps of the study area obtained from airborne geophysical data of the GTK and gravity data of the FGI. Location of the studied area is indicated in Figure 1. (a) A map of apparent resistivity of the bedrock calculated by the joint inversion of airborne electromagnetic and static magnetic data (Pirttijärvi et al., 2014). (b) A grayscale map of low-pass filtered aeromagnetic data after reduced to the pole (Korhonen, Aaro, All, Elo, et al., 2002). (c) A Bouguer anomaly map from gravity measurements by FGI and GTK (Korhonen, Aaro, All, Nevanlinna, et al., 2002). The color-coded lines represent the lineaments along gradients in the CFGC (red), the outer part of the VMC (white), the inner parts of the VMC (blue), the offshore zone (black). (d) Rose diagrams shows the division of the lineaments in the VMC and the CFGC.

and magnetotelluric profiles (BABEL Working Group, 1990; Korja & Heikkinen, 2005; Kukkonen et al., 2006; Korja et al., 2013; Vaittinen et al., 2012). Altogether, the geophysical data can be used to constrain tectonic and geodynamic evolution models of the study area.

2.2. The VMC

The VMC (Figure 2) is situated within the Pohjanmaa schist belt (Nironen et al., 2002). It consists of supracrustal rocks that have been deformed, metamorphosed, and partially molten during the Svecofennian orogeny (Kähkönen, 2005; Mäkitie et al., 2012). The complex is bordered by the Quark shear zone to the south (Korja & Heikkinen, 2005) and by the Soini shear zone to the east. Based on the progressive increase of LP-HT metamorphic grade from amphibolite to granulite facies (e.g., Alviola et al., 2001), the VMC can be divided into outer and inner parts. The outer part (Bothnian schist belt; Kousa & Lundqvist, 2000) comprises mainly metasedimentary schists, gneisses, and metatexitic migmatites, whereas the inner part (also known as Vaasa Batholith or Vaasa granite) comprises diatexitic migmatites and anatectic S-type granitoid rocks such as granite and granodiorite (Mäkitie et al., 2012).

The supracrustal rocks of the Pohjanmaa schist belt are part of the lower Svecofennian stratigraphic unit (or western Finland supersuite; Luukas et al., 2017) defined by Lundqvist et al. (1996). Based on the analysis of detrital zircons, Lahtinen et al. (2002, 2017) have proposed a maximum deposition age of 1.92–1.91 Ga for this stratigraphic unit. The western part of the Pohjanmaa schist belt (Lappfors suite) is mainly composed of turbiditic pelites and greywackes with scarce carbonates and calc silicates. Intercalations of mafic volcanic units (low-K subalkaline basalts and basaltic andesites) and associated black schists are found in the southeastern part (Pirttikylä suite) of the belt. The mafic intercalations are of mid-oceanic ridge and within plate affinities (Kähkönen, 2005; Vaarma & Kähkönen, 1994; Vaarma & Pipping, 1997) suggesting rift-related origin (Lahtinen et al., 2017; Vaarma & Kähkönen, 1994). In the work by Williams et al. (2008), the Lappfors suite is interpreted as a pre-1.92 Ga marginal basin subsequently affected by extension and associated deposition of the Pirttikylä suite at ∼1.91–1.90 Ga. Early deformation and metamorphism with unknown origin might have preceded the deposition of the Pirttikylä suite at ca. 1.92–1.91 Ga (Lahtinen et al., 2017; Williams et al., 2008).

Based on field work and petrological and geochemical observations of the VMC granitoids in the inner part and the surrounding migmatites and schists in the outer part, Mäkitie (2001) suggested that the granitic rocks represent in situ melting of the adjacent sedimentary rocks. This is supported by the similar inherited U-Pb ages, the initial Nd isotopic composition of the granitoids, and the surrounding metasediments (Kotilainen et al., 2016b; Suikkanen et al., 2014). The initial ε_{Nd} values of the granitoids are consistently slightly negative, around −2, implying a large component of recycled continental material in the source (Suikkanen et al., 2014). Both the granitoids (mostly granites and granodiorite) and the diatexites of the inner part are peraluminous, calc-alkalic to alkali-calcic and magnesian, enriched in Light Rare Earth Elements (REEs) with a moderate to strong REE fractionation, mostly minor negative Eu anomaly, and with a distinct spread in the heavy REE contents (e.g. Kotilainen et al., 2016a; Mäkitie et al., 2012).

Most of the magmatic U-Pb zircon ages from the igneous rocks of the VMC fall in the range of ~1.88–1.86 Ga, and the monazite are cluster at ~1.87–1.86 Ga (e.g., Kotilainen et al., 2016b; Suikkanen et al., 2014). There seems to be indefinite pattern in the spatial distribution of the ages. The central inner parts of the complex tend to display younger zircon crystallization ages than those further away from the center (Kotilainen et al., 2016b), and age difference between the zircon and monazite ages grows toward the center of the VMC (Kotilainen et al., 2016a). It is interpreted to indicate progressively slow cooling from the margin to the center of the VMC (Kotilainen et al., 2016a). There are no U-Pb concordia zircon age data available from the mica schists in the outer part of the VMC, but the zircons from both the xenolith schists and from the VMC granitoids give metamorphic ages of 1.88–1.86 Ga, similar to the magmatic U-Pb ages in the area (Kotilainen et al., 2016b).

Although the tectonic evolution of the VMC is poorly known, ENE- to E-directed transport (recumbent folds and thrusts) of the supracrustal rocks has been suggested by Vaarma and Pipping (1997). The descriptions of the HT-LP metamorphic zones (Alviola et al., 2001; Hölttä & Heilimo, 2017; Lehtonen et al., 2003; Mäkitie et al., 2001; Mäkitie & Lahti, 2001; Vaarma & Pipping, 1997) highlight the increase of the metamorphic grade

from the outer parts to the inner parts of the VMC. There is a gradual transition from andalusite/staurolite schist to sillimanite + cordierite gneiss and to metatexites in the outer part, toward diatexites and aluminium-enriched S-type granitoid plutons in the inner part (Mäkitie et al., 2012, and references therein). The equilibrium temperature of migmatites is bracketed at 600–720 °C at about 5 kbars based on conventional geothermometers (garnet-cordierite) (Lehtonen et al., 2003). This paroxysmal tectonothermal event has taken place at 1.88–1.87 Ga (Korsman et al., 1999; Kotilainen et al., 2016a, 2016b; Mäkitie et al., 2012; Suikkanen et al., 2014). During postorogenic event at ca. 1.80–1.79 Ga, REE pegmatites have intruded the outer part of the VMC (Alviola et al., 2001, and references therein).

3. Geophysical Features of the VMC

3.1. Geophysical Maps

Low-altitude (30 m) airborne geophysical data by courtesy of the Geological Survey of Finland and Bouguer anomaly gravity data by courtesy of the National Land Survey (Finnish Geodetic Institute) are presented in the form of an apparent resistivity, an aeromagnetic, and a Bouguer anomaly maps (Figure 3; for more detailed descriptions of the data, see Leväniemi et al., 2009; Korhonen, 2005; Korhonen, Aaro, All, Elo, et al., 2002). The maps have been used to draw km-scale structures that have been verified in the field.

The apparent resistivity map (Figure 3a) is the result of two-layer joint inversion of the in-phase and out-of-phase components of the airborne electromagnetic and static magnetic field data (Pirttijärvi et al., 2014). Conductors are colored in red tones and the background resistive areas in white. Most of the conductors have linear forms following the more conductive black schists and basaltic units, which form local anomaly maxima in the high resistivity background composed of turbiditic metasediments. The conductive linear anomalies follow roughly the trend of the Pirttikylä suite, which forms a 50 km wide belt. It is limited in the west by the more resistive Lappfors suite and the igneous rocks of the VMC and in the east by the highly resistive CFGC. In the southern part, an E-W trending linear zone of high conductivity coincides with surface outcrops of the Quark shear zone.

Aeromagnetic data are imaged as a grayscale map (Figure 3b) displaying low-pass filtered magnetic anomalies reduced to the pole. The intensities of the magnetic anomalies are controlled by the amount of magnetic minerals in rocks. The magnetic mafic volcanic rocks and black schists form several, semiparallel linear anomaly maxima in the weakly magnetic background composed of mica schists, migmatites, and granitoids. The latter are displayed as homogenous, featureless magnetic minima. The broad belt of E-W trending minima and maxima coincides with the Quark shear zone at the southern boundary of the VMC (Figure 2). In the inner part of the VMC, minor anomalies surround several semicircular areas that correspond to magmatic domes (geomagnetic areas in Kotilainen et al., 2016b). In a more detailed map view (Figure 3b, inset), the high amplitude magnetic anomalies outline a km-scale E-W folding of originally N-S striking lithologic units.

The regional Bouguer anomaly map is based on the Fennoscandian Bouguer anomaly data of National Land Survey and Geological Survey of Finland (Korhonen, Aaro, All, Nevanlinna, et al., 2002) defined on a 2.5 km by 2.5 km grid. The absolute Bouguer anomaly values range from −60 to 20 mGal within the study area (Korhonen, Aaro, All, Nevanlinna, et al., 2002). Figure 3c is a residual map after applying a high-pass filter to remove long wavelength anomalies originating from deeper parts of crust. Lineaments that follow major gradient changes have been extracted manually from the residual map. They have been used as input data for the rose diagrams on direction of lineaments in different parts of the study area (Figure 3d). The Bouguer anomaly lineaments show a weak E-W trending pattern in the CFGC and the inner part of the VMC and a strong E-W trending pattern in the outer part of the VMC.

All the three types of geophysical maps (apparent resistivity, magnetic, and residual Bouguer anomaly) show three contrasting geophysical domains in the study area and inner and outer parts of the VMC and CFGC. The inner part is characterized by the lack of conductivity anomalies, subcircular regions lacking magnetic anomalies and large variation in direction of the Bouguer anomaly lineaments. The outer part of the VMC is characterized by high magnetic and conductivity maxima as well as strongly E-W aligned Bouguer anomaly lineaments. The CFGC is characterized by the lack of conductivity anomalies, rather chaotic pattern of low and high amplitude magnetic anomalies and rather bimodal distribution of Bouguer anomaly lineaments

expressed by weak NE-SW and strong E-W maxima in the corresponding rose diagram (Figure 3d). The southern zone, which broadly parallels the Quark shear zone, shows magnetic, resistivity, and Bouguer anomaly lineaments preferentially aligned in WNW-ESE direction (Figures 3c and 3d). The magnetic map suggests that the general E-W trend of the anomalies results from the regional folding of the originally N-S trending lithological boundaries (Figure 3b, inset).

3.2. Seismic Reflection Profiles

Deep seismic reflection data are used to outline the crustal-scale structural architecture. The near vertical reflection data are the migrated normal move out data from FIRE 3a profile (Korja & Heikkinen, 2005, 2008; Kukkonen et al., 2006) transecting the VMC and the CFGC (Figures 2 and 4). The data are displayed as an instantaneous amplitude section and an automatic line drawing (Figures 4a and 4b). In the instantaneous amplitude section, the data are average both horizontally and vertically and plotted as grayscale intensities (for technical details, see Korja & Heikkinen, 2005; Kukkonen et al., 2006). The instantaneous amplitude section highlights changes in reflectivity between different blocks, whereas the automatic line drawing highlights the apparent dip of the reflections (Figure 4b). Seismic reflections stem from lithological contacts with large velocity and density contrasts. In highly metamorphosed and deformed areas, lithological contacts can either be primary or tectonic. Weak reflectivity indicates a rock mass with weak density-velocity contrasts, for example, monotonous intrusions and older crustal pieces in which the internal structure has been homogenized in the scale of reflectivity.

The zone of strong reflections dipping gently to the SE in the middle crust is interpreted to image an accretionary system. In the NW part, a highly reflective block in the lower crust (distances 0–60 km) may represent a crustal block that has been underthrust beneath the accretionary belt (Korja & Heikkinen, 2008; Korja & Heikkinen, 2008; Korja et al., 2009; Lahtinen et al., 2009; Kukkonen et al., 2006; Sorjonen-Ward , 2006).

3.3. Magnetotelluric Profiles

Broadband magnetotelluric data (MT) are used to outline the deep structure and to resolve the amount of sedimentary material at depth and granitoid plutons at surface (e.g., Rao et al., 2007). MT data used in this study are from two new parallel profiles, MT-PE and MT-B2, across VMC and CFGC (Figure 2). MT-PE has been acquired along the same path as the seismic reflection profile FIRE 3a. Geoelectric dimensionality and strike analyses (Smirnov & Pedersen, 2009) applied for these data show that MT data appear to be two-dimensional in the shortest periods. At longer periods, the data show three-dimensional regional behavior and thus precluding the modeling of the upper mantle without a full three-dimensional inversion. In addition, the analysis of all measured MT data reveal a regional trend of azimuth 55°. Thus, before modeling the MT data, the sites have been projected to new profiles perpendicular to the strike (N35°W). The MT data have been inverted using the two-dimensional inversion code REBOCC from Siripunvaraporn and Egbert (2000).

The final inversion models between 0 and 70 km in depth along profiles MT-PE and MT-B2 are shown in Figures 4c and 4d, respectively. The modeled data yield a good fit to the observed data (root mean square equals 1.3 and 1.0, respectively). The profiles image a highly resistive eastern part at CFGC, with the total conductance of a few tens of Siemens, and a highly conducting western part at VMC, with the conductance in the range of tens of thousands of Siemens. The deep conductors can be traced close to surface, where near-surface conductivity anomalies are observed by airborne electromagnetic measurements (see Figure 3a). The conductive structures in the western part of the VMC have been tested using several a priori models (not reproduced here) on both profiles. The tests show that the deep conductors are more likely thin and compact layers with high conductivity (such as graphitic black schists from the Pirttikylä suite at surface) rather than thick layers with lower conductivity values.

4. Structural Geology of the VMC

We attempt to provide a plausible explanation via structural and petrological analyses for the geophysical patterns deduced from both the surface geophysical maps and the deep geophysical profiles. We will outline finite structural pattern (Figures 5–8) and crustal-scale metamorphic zones that can be redefined further using P-T data (Figure 9). The structural observations on the structural map of the VMC (Figure 5) are

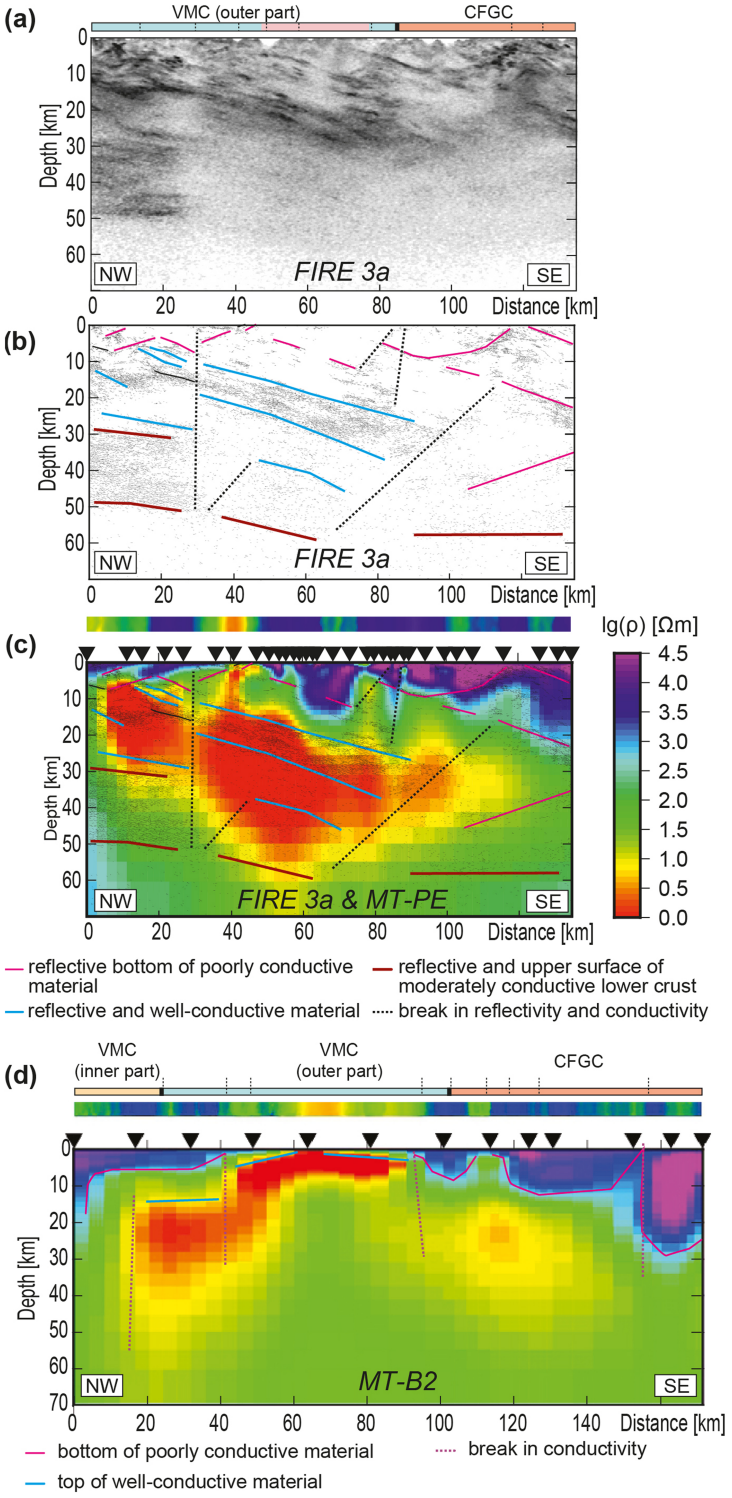

Figure 4. Crustal structure of the VMC along FIRE 3a deep seismic reflection profile and along MT-PE and MT-B2 magnetotelluric profiles. No vertical exaggeration. The location of the profiles is shown in Figure 2. Uppermost panels show the lithological units and major shear zones derived from Figure 1. Structural interpretations are derived from the reflectivity and conductivity anomalies of the crustal units. (a) An instantaneous amplitude section of FIRE 3a displayed as grayscale intensities (after Korja & Heikkinen, 2008). (b) An automatic line drawing of seismic reflectivity data along FIRE 3a profile (Korja & Heikkinen, 2008) and a color-coded structural interpretation. (c) A color-coded resistivity model from the 2-D inversion of magnetotelluric determinant data along MT-PE profile (after Vaittinen et al., 2012) is overlain by Figure 3b. The horizontal strip shows the apparent resistivity at surface (Figure 3a). Inverted triangles refer to the locations of the MT sites. (d) A resistivity model from 2-D inversion of MT data along profile MT-B2 and a structural interpretation. The horizontal strip shows the apparent resistivity at surface (Figure 3a). Inverted triangles refer to the locations of the MT sites.

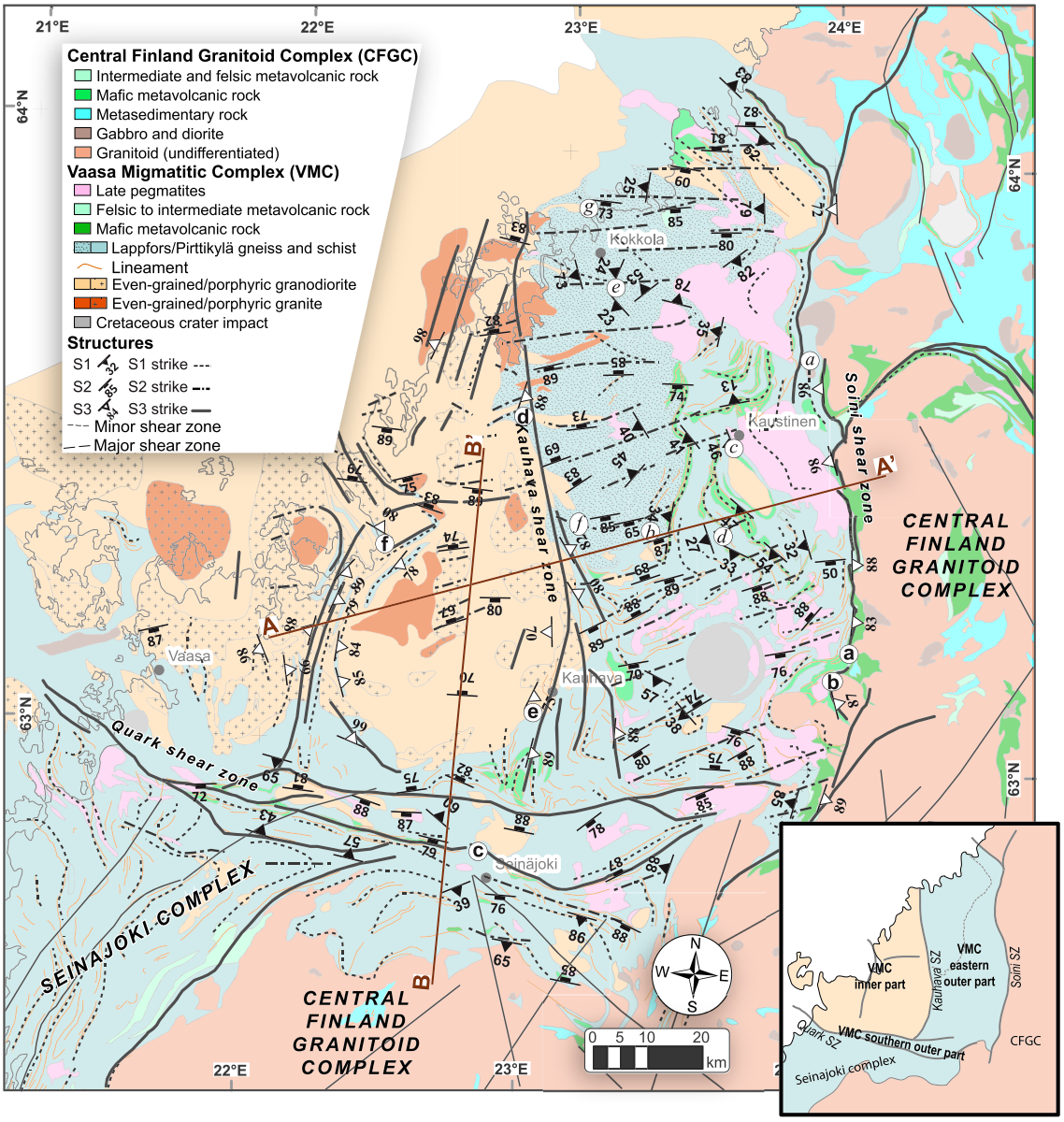

Figure 5. A structural map of the Vaasa migmatitic complex. The red line segments A-A′ and B-B′ locate the block models in Figure 6. The letters in italic (a–g) and in bold (a–f) with white background circles locate the photographs in Figures 7 and 8, respectively.

based on extensive field work, whereas the shear zones are interpreted from the digital bedrock map 1:200,000 © Geological Survey of Finland (2012) and from anomalies on the aeromagnetic map (Figure 3b). The VMC can be divided into three main structural zones: (1) the eastern and (2) the southern outer part with mica schists and metatexites and (3) the inner part with diatexites and granitoids. With the help of the structural map (Figure 5) and two block models (Figure 6) and field photographs (Figures 7 and 8), we have identified three main deformation structures (D1–D3) with variable intensity and geometry. The D1 forms shallow to moderately dipping metamorphic foliation S1. The D2 corresponds to a regional N-S shortening responsible for the formation of ~E-W striking upright folds associated with axial planar cleavage S2. The D3 corresponds to subvertical shear zones observed inside and along the border of the complex.

4.1. The Eastern Outer Part of the VMC

The metamorphic foliation S1 is generally parallel to the lithological layering S0 (Figures 7a and 7b; e.g., sedimentary bedding and mafic volcanic layers), but axial planar cleavage S1 is also observed in some

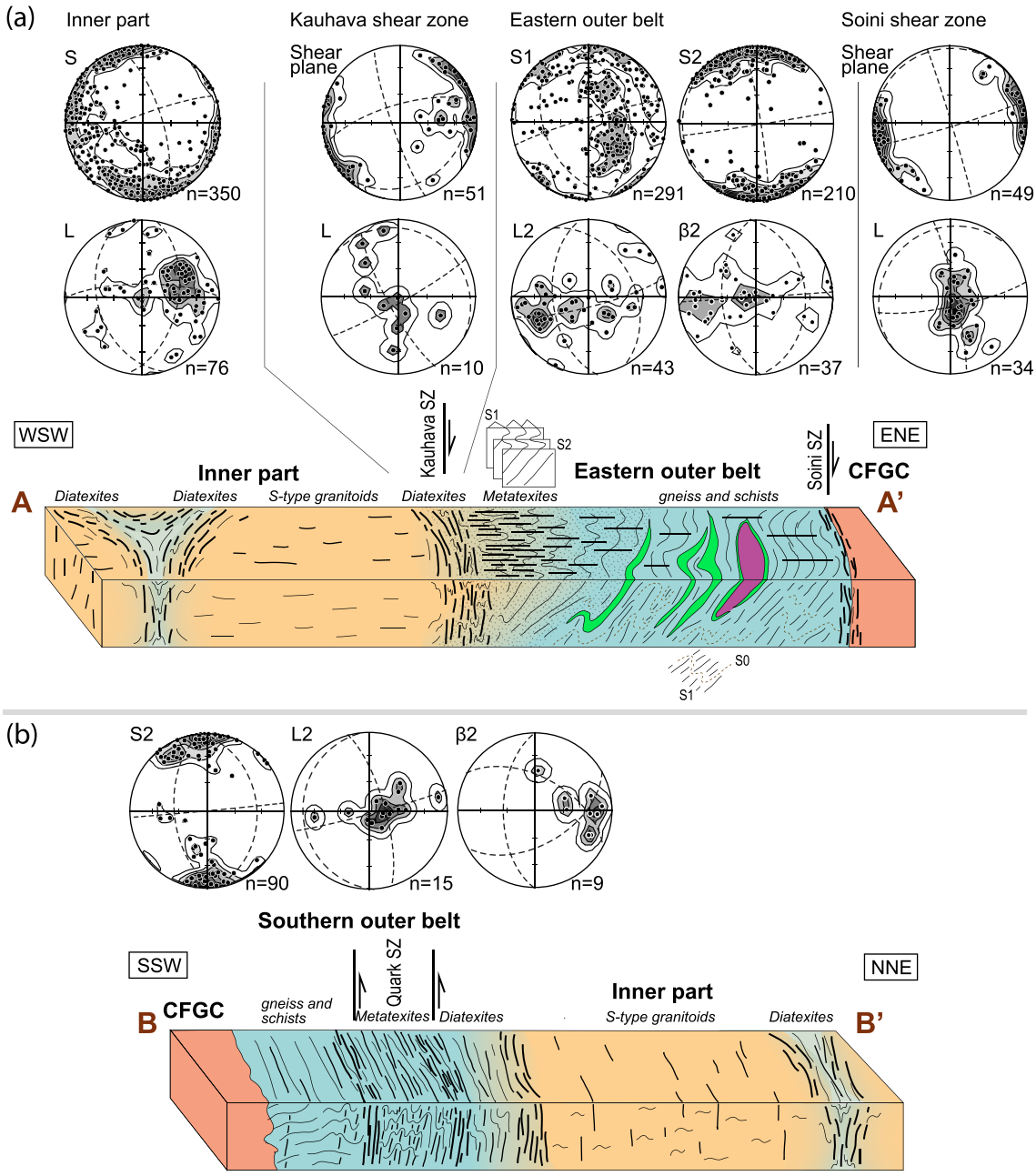

Figure 6. Schematic block models (see location in Figure 5) and stereographic diagrams (equal-area, lower hemisphere projections) of planar and linear structures.

outcrops (Figure 7c). The foliation S1 is well preserved in the mica schists from the eastern part of the belt where it is generally moderately dipping toward the W-SW with mineral and intersection lineations plunging in the same direction (Figures 5, 6a, and 7d). In the central and western parts, a well-developed West dipping gneissic layering S1 is observed in stromatic metatexites (Figures 6a and 7e). S1 is heterogeneously affected by D2 E-W trending upright folds (Figures 5 and 6a). In the easternmost part, moderately westward plunging, open F2 folds of 5–10 km wavelength are visible at map scale, marked by the bending of layers of mafic metavolcanic rocks (Figures 5 and 6a). The development of a new S2 axial planar foliation at the outcrop scale is quite rare, however. The intensity of F2 folding is stronger in the metatexites where close to isoclinal upright folds are widespread (Figure 7e). A new WSW-ENE vertical axial planar migmatitic foliation (S2) is formed (Figure 7f), bearing a weak vertical to moderately west

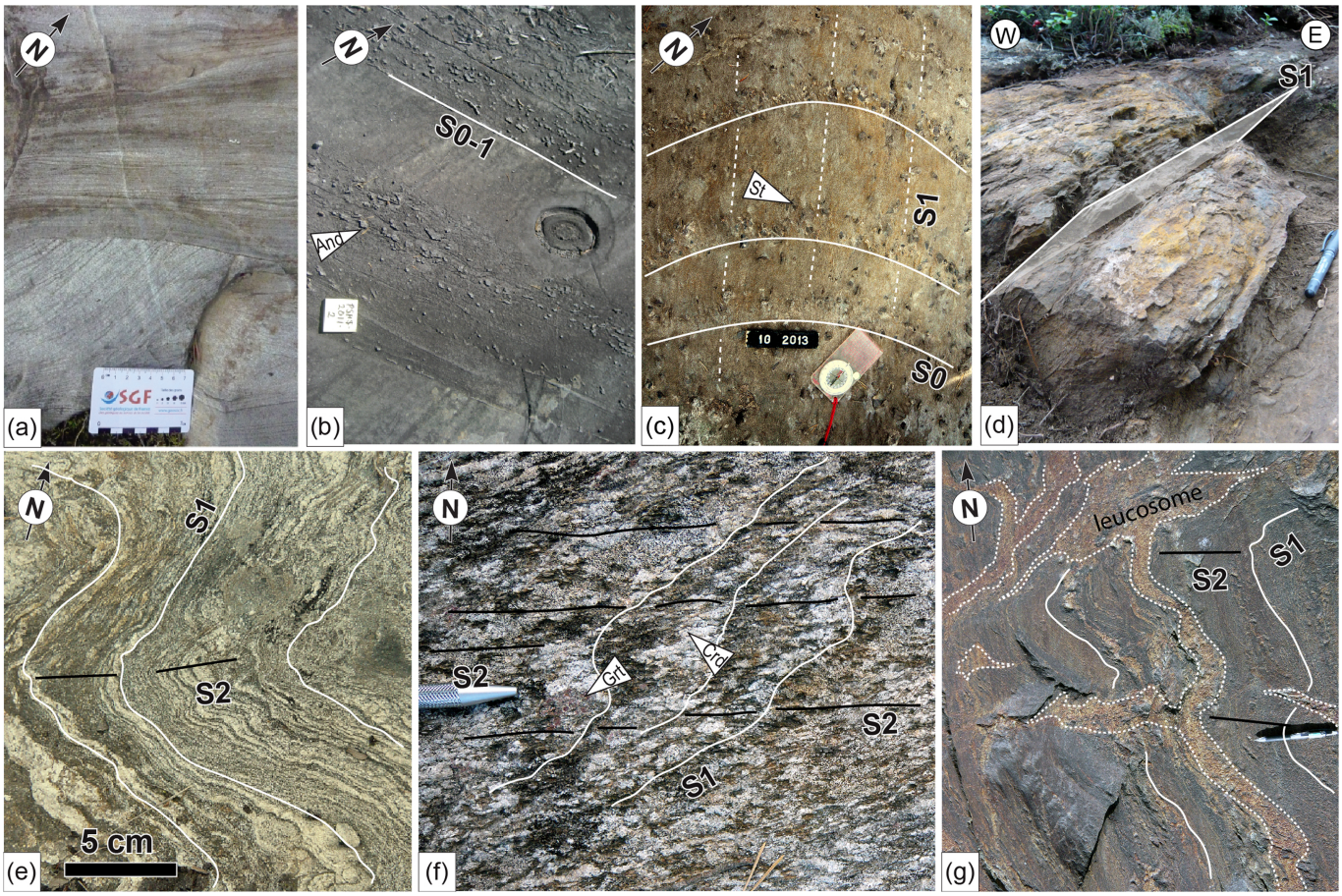

Figure 7. Field photographs from the eastern outer part of the VMC. (a) Well-preserved cross-bedding in a metaarkose from the staurolite zone (Ia). (b) Bedding made by an alternation of metapelite and metasandstone from the andalusite zone (Ib). A calc schist concretion on the right is visible. The dots are pseudomorphes of andalusite after white micas. (c) Open F1 fold in a staurolite-garnet bearing mica schist. (d) West dipping S1 schistosity in a graphite bearing mica schist. (e) Westward plunging open to close upright F2 fold in a stromatic metatexite. (f) Axial planar, E-W striking subvertical S2 schistosity in a stromatic metatexite. Crd are oriented parallel to S2. (g) Percolation of leucosomes into the axial plane of F2 folds. See Figure 5 and Table S1 for the location of the photographs.

dipping mineral and intersection lineation (L2), parallel to the fold axes (Figure 6a). The axial plane is generally filled by leucosomes (Figure 7g). In some places, it completely transposes older (S0-1) foliation (Figures 5 and 6a).

The eastern border of the VMC is intensively reworked by the 200 m wide noncoaxial, subvertical N-S striking Soini shear zone (Figures 5 and 6), which marks the contact between the VMC and the CFGC (Nikkilä et al., 2015). The deformation zone reworks supracrustal rocks and gneissic granitoids and shows strong fabric with subvertical foliation and lineation (Figure 8a). A west-side up kinematic is inferred from the observation of S-C(-C′) fabrics (Berthé et al., 1979) in some augen orthogneiss (Figure 8b).

4.2. The Southern Outer Part of the VMC

The southern outer part of the VMC bears strong similarity with the eastern outer part. The metamorphic foliation S1 in the mica schists and metatexites is strongly affected by F2 event (Figures 5 and 6b). In map view (Figure 5), E-W striking kilometric F2 folds are well visible south of town of Vaasa. In the field, the D2 is observed from eastward plunging upright open to close folds (Figure 8c) and E-W striking axial planar schistosity S2 bearing a weak to moderate subvertical mineral lineation L2 (Figure 6b). The folding and cleavage are geometrically coherent with the Quark shear zone. Despite the presence of a strong vertical mineral lineation in some places, the kinematics remains unclear (see also Mäkitie et al., 2001). Interpretation of the aeromagnetic map (Figure 3b) suggests that Quark shear zone is an E-W striking subvertical deformation zone, which separates migmatites to the north from mica schists intruded by granitoids in the south.

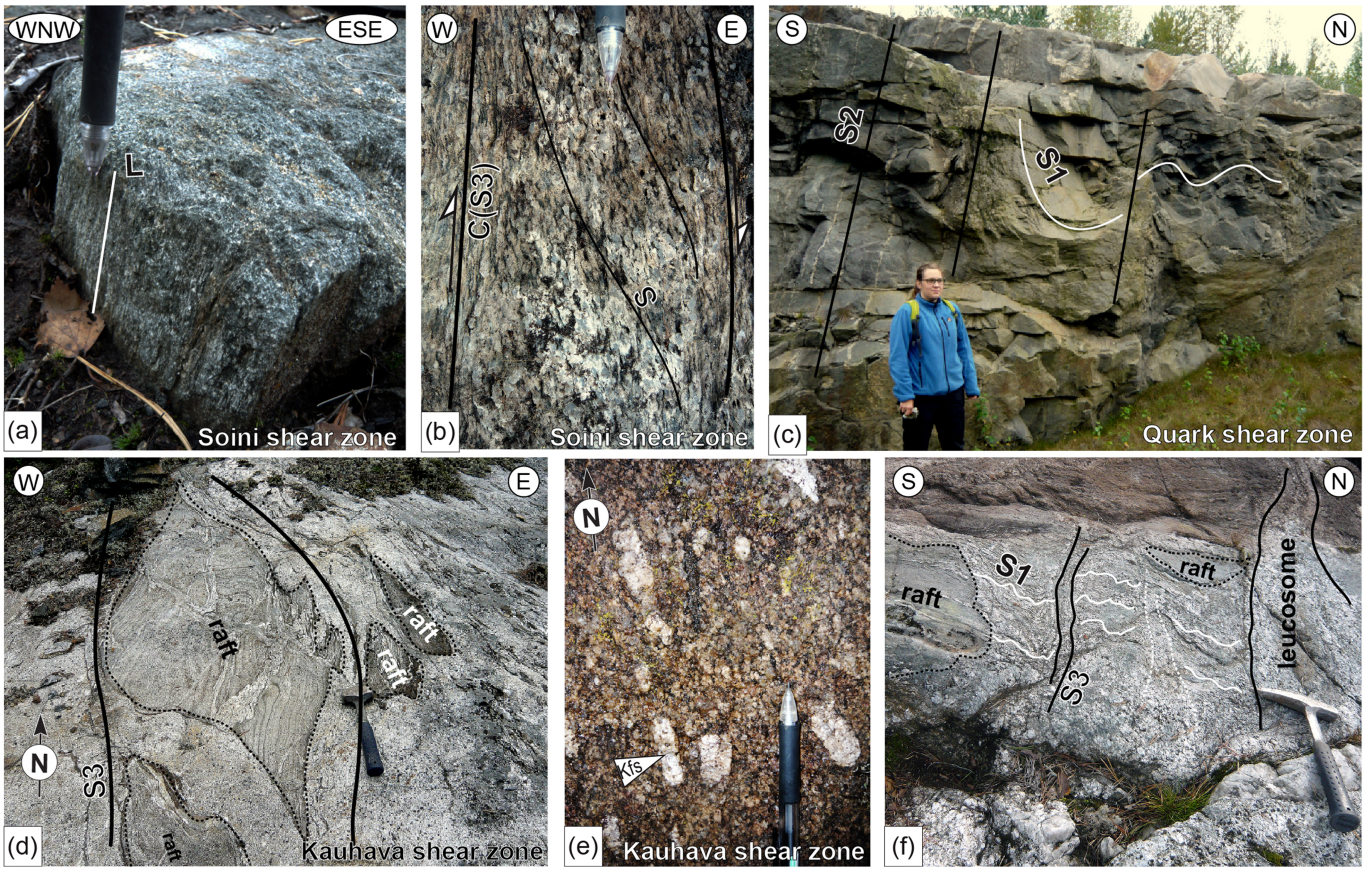

Figure 8. Field photographs from the Soini, Quark, and Kauhava shear zones and from the inner part of the VMC. (a) N-S striking mylonitic amphibolite showing subvertical foliation and lineation. (b) C-S structure (upward movement of the western block) affecting a granite within the subvertical Soini ductile shear zone (XZ section of the finite strain ellipsoid). (c) E-W striking upright open F2 folds in metatexites migmatite from the Quark shear zone. (d) N-S striking, subvertical-sheared diatexites migmatites with raft of metatexites migmatite near Kauhava. (e) Preferred orientation of Kfs phenocryst in a porphyric granitoid. (f) Folded diatexite in the inner part of the VMC. See Figure 5 and Table S1 for the location of the photographs.

4.3. The Inner Part of the VMC

The interpretations of the lithological and aeromagnetic maps, together with the structural observations, suggest that the inner part of the VMC comprises three subrounded domes mainly composed of granitoids and separated by diatexites (Figures 3b, 5, and 6). The structure of the granitoids is generally isotropic, but in some places, they show a subhorizontal to a WSW-ENE striking subvertical foliation (Sipilä et al., 2008) nearly parallel with the strike of S2 in the outer parts of the VMC (Figures 5 and 6). The main S3 foliation in diatexites is vertical and follow the border of the subrounded zones (Figures 5 and 6), for example, along the Kauhava shear zone (Figures 8d and 9e), although an earlier subhorizontal foliation, affected by open and upright folds, is observed (Figure 8f). The D3 structures are interpreted as vertical deformation zones in diatexites in between and around subrounded granitoid domes.

5. Metamorphism of the VMC

5.1. Metamorphic Zones

The metamorphic zones in the VMC are presented in the Figure 9a (modified after Hölttä & Heilimo, 2017). Because rock units in the VMC are mostly of metasedimentary origin, the metamorphic zones are constructed on the basis of the observed mineral assemblages in Al-rich metasedimentary rocks. Other factors used in the metamorphic classification are the preservation of primary sedimentary structures, the grain size, and the onset and degree of melting. Mineral abbreviations in the text and in the figures follow the IUGS recommendations

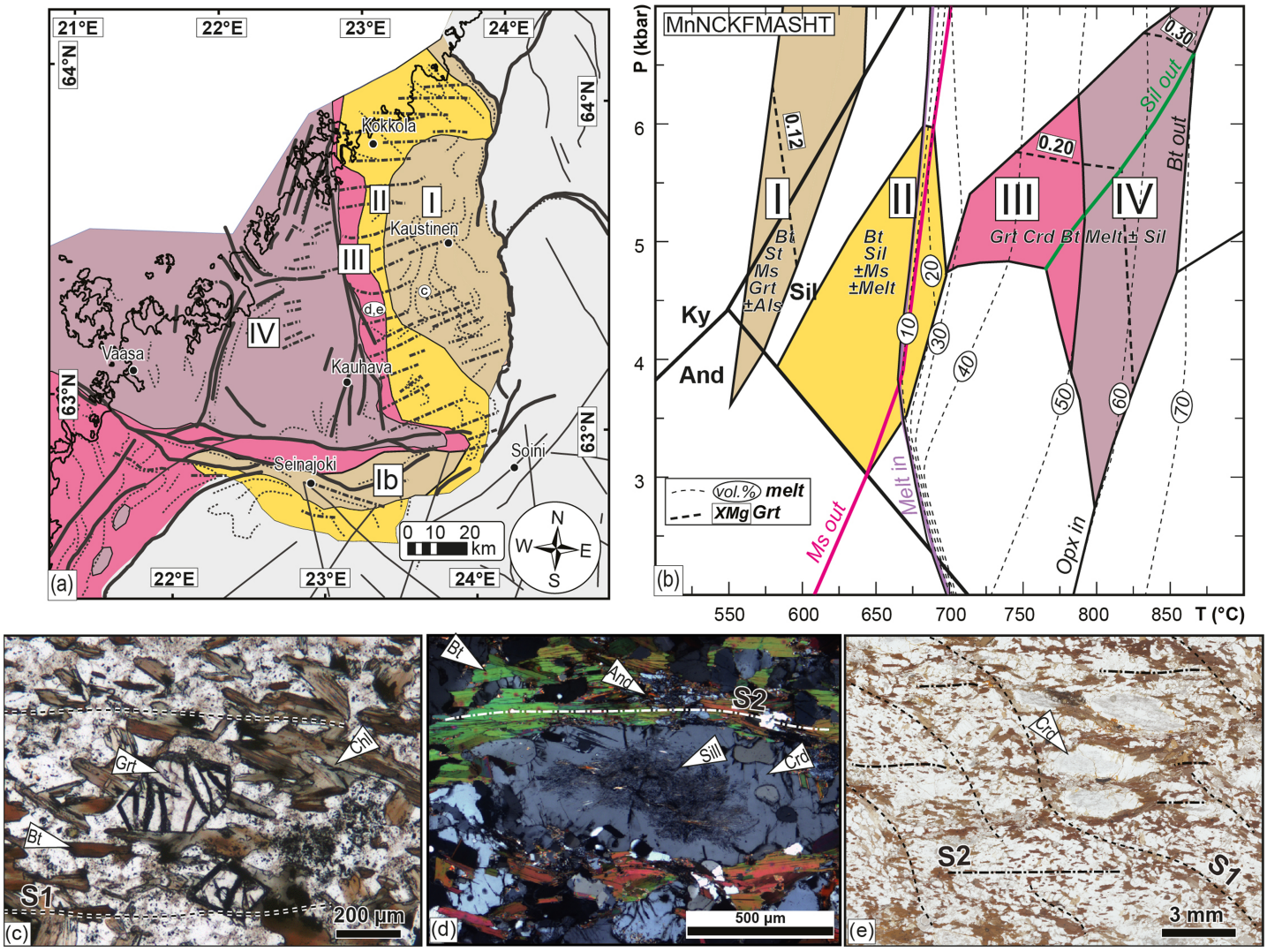

Figure 9. Metamorphism of the VMC. (a) A metamorphic map of the VMC showing the different metamorphic zones. (background) Structures from the Figure 5. (b) A simplified pseudosection for a representative Al-rich pelitic rock (modified after Hölttä & Heilimo, 2017, where reference to the whole rock composition can be found). (c) Grt-Bt mica schist from the garnet-staurolite zone (plane-polarized light). (d,e) Crd-Grt metatexite from the metatexitic garnet-cordierite zone. The location of the photographs is shown on (a) and in Table S1.

(Siivola & Schmid, 2007): plagioclase (Pl), K-feldspar (Kfs), muscovite (Ms), biotite (Bt), staurolite (St), garnet (Grt), aluminosilicate (Als), kyanite (Ky), andalusite (And), and sillimanite (Sil).

Figure 9b is a simplified PT pseudosection (modified after Hölttä & Heilimo, 2017) constructed using a composition of an Al-rich, high-K, and low-Ca metapelitic rock representative of the study area. The subsolidus part is calculated with excess SiO_2 and H_2O, assuming that dehydration reactions keep the system H_2O saturated and the suprasolidus part is calculated assuming excess in SiO_2 and H_2O = 3.0 wt.%. The diagram shows the approximate changes in PT only in the fields of the common observed mineral assemblages. Colors in the pseudosection correspond to the colors of the metamorphic map in Figure 9a. Although the stability fields for mineral assemblages on the pseudosections are sensitive to the whole-rock composition, they give approximate PT limits for each metamorphic zone mapped in the field. The melt volumes presented on the pseudosection are the maximum volumes that can be produced from this composition.

Four metamorphic zones are distinguished in the area (Figures 9a and 9b): (I) the garnet-staurolite zone, (II) the sillimanite-melt zone, (III) the metatexite garnet-cordierite zone, and (IV) the diatexite garnet-cordierite

zone. Here, an attempt is made to correlate the mineral growth and development of previously described structures.

In the garnet-staurolite zone (Zone I), metasedimentary rocks show well-preserved sedimentary structures (Figure 7a), and metapelitic rocks are fine-grained schists. In Al-rich schists, the S1 schistosity is defined by the mineral association Qtz + Pl + Mu + Bt ± Grt ± St ± Als. The aluminosilicates are mostly andalusite porphyroblasts (Figure 7b), but fibrolitic sillimanite prevails in the western part of the zone. Porphyroblasts of staurolite and garnet may be up to 1–2 cm in size (Figures 7c and 9c). Some staurolite porphyroblasts have been replaced by cordierite. When visible, the S2 cleavage contains mica laths. During retrogression, biotite is chloritized and andalusite pseudomorphosed by muscovite.

In the sillimanite-melt zone (Zone II), metasedimentary rocks are medium-grained gneisses with the association Bt + Qtz + Pl + Ms + Bt ± Grt ± Sil ± Kfs in the S1 fabric. Commonly, the gneisses have 1–5 vol.% of narrow leucosome layers and patches indicating the onset of partial melting during D1 (Figure 7e). S2 cleavage shows secondary micas and presence of leucosome.

In Zone III, the metasedimentary rocks are medium-grained metatexites with ~5–20 vol.% leucosome (Figure 7f), which is less than predicted in Figure 9b for a pelitic composition. This may be partly due to melt loss but is also caused by the fact that outcrops normally represent alternating pelitic and psammitic layers or psammites only, psammitic compositions producing much less melt than pelites in the same PT conditions. Common mineral associations in the metapelites are Bt + Qtz + Pl + Bt + Grt + Crd + Sil ± Kfs. In the Zone III, the abundance of garnet is minor but increases toward Zone IV. Sillimanite is commonly found as inclusions in cordierite and garnet (Figure 9d), indicating that it was a reactant in the melting reaction Bt + Sil + Qtz = Grt + Crd + melt. Sillimanite inclusions in cordierite delineate the S2 schistosity (Figures 7f and 9e), and leucosomes are in F2 axial planes suggesting that this melting reaction was still active with D2 (Figure 7g). Small andalusite ± kyanite grains are found as retrograde phases after cordierite and biotite (Hölttä & Heilimo, 2017) along the S2 foliation.

In Zone IV, the rocks are mostly represented by schlieric diatexites (Figures 8d and 8f) with up to 50–80 vol.% leucosome and S-type granitoids (Figure 8e). Some mesosomes have the association Grt + Crd + Bt + Pl + Qtz ± Kfs ± Sil, but commonly, the mesosomes have the assemblage Bt + Pl + Qtz ± Grt. Like in Zone III, sillimanite is found as inclusions in cordierite, which in turn is replaced by andalusite during retrogression.

5.2. PT Conditions

Based on the pseudosection in Figure 9b, the rough estimates for metamorphic temperatures for each zone indicate an increase from ~550–600 °C in Zone I to ~780–850 °C in Zone IV. Metamorphic conditions of 3.5–4.5 kbars and 570 °C are estimated in St-Grt-And-bearing metapelites from the eastern border of the VMC in Zone I (see also Hölttä & Heilimo, 2017). Zircon and monazite saturation temperatures from the granitoids of Zone IV fall in the 805–875 °C range (Kotilainen et al., 2016a). Figure 9b shows selected X_{Mg} isopleths of garnet, ranging from 0.20 to 0.30 in Zones III and IV (Mäkitie et al., 2001). These garnet compositions together with the observed mineral paragenesis suggest a range of pressure from 3.5–4.5 kbars in Zone I to 5.5–7 kbars in Zone IV in the sillimanite stability field (Figure 9b). Nevertheless, especially in Zone IV, sillimanite is found only as inclusions in garnet and cordierite (Figure 9e) implying that the biotite melting reaction consumed sillimanite from the rock matrix with increasing temperature. Above the sillimanite field in biotite-bearing rocks, garnet and cordierite compositions are mainly controlled by temperature (Figure 9b), and consequently, the pressure could have been as low as ~4 kbars. Commonly found retrograde reactions, staurolite, and andalusite in migmatites indicate cooling down to ~550 °C and 3.5–4.5 kbars (Figure 9b). It corresponds to the X_{Mg} of 0.58–0.65 of cordierite from the Zones III and IV in the inner part of the VMC (Lehtonen et al., 2003) where diffusion could have modified their composition during cooling. These data are only appropriate for the first-order quantification of the metamorphic conditions, and more detailed petrological analysis are needed.

6. Discussion

The geophysical data (Figures 3 and 4) together with the structural and metamorphic observations (Figures 5–9) suggest a three-stage tectonic evolution of the VMC. The first stage is the development of the main metamorphic fabric S1 related to the eastward thrust of hot orogenic core. The second stage is

lateral N-S shortening associated with upright folding and development of new vertical E-W striking metamorphic schistosity S2. The third stage is the vertical transfer of hot orogenic core along steep shear zones. The evolution stages can be correlated with important crustal orogenic processes such as horizontal flow of hot fold nappe as part of accretionary prism dynamics (Beaumont et al., 2006) followed by crustal-scale oroclinal buckling (e.g., Weil et al., 2019) terminated by buoyancy-dominated flow (e.g., Kruckenberg et al., 2011) of hot and partially molten material in an orocline hinge.

6.1. Geological Interpretation of the Geophysical Cross Section: Continuity Between Surface Geology and Geophysical Data

The geophysical signal deciphers the exposed lithological units, in particular the boundaries between granitoids (inner part of VMC and CFGC) and supracrustal rocks: schists, gneiss, and metatexites (outer part of VMC). The supracrustal rocks are divided into poorly conductive, conductive, and highly conductive (graphite-rich) ones.

Along the FIRE 3a seismic and MT-PE magnetotelluric profiles (Figure 4), the moderately reflective, poor to moderately conductive upper crust of the VMC shows subhorizontal to shallow NW or SE dipping reflections. The reflections have been interpreted as primary contractional (Sorjonen-Ward, 2006). Similarly, because no late detachment zones or vertical shortening are reported in the VMC, we can postulate that the main reflections in the seismic profiles are likely early fabrics originated from lithological boundaries reworked during D1. Field observations show that S1 metamorphic foliation is dipping moderately to the W-NW along the profile, which is coherent with the two-dimensional geophysical observations (upper crustal level). Poorly conductive blocks are associated with outcropping granite at surface. In some areas moderately enriched in graphite at surface, such as the Lappfors suite of the VMC, the conductivity may be decreased by the wealth of granitoid plutons (Veteli and Kaustinen intrusions) (Figure 10a). In the NW part of the profile (distances 0–80 km), at the middle and lower crustal levels, southeastward dipping, highly reflective and highly conductive middle crustal block is placed on the top of moderately conductive and less-well reflective lower crust. The high conductivity and reflectivity could be explained with the presence of a 20–30 km stack of graphite-bearing supracrustal material, similar to the Pirttikylä suite, on top of a downgoing lower crustal block (Bothnian microncontinent; Lahtinen et al., 2005). In the SE part of the MT-profile (distances 80–130 km), the conductivity pattern in the upper 10–25 km is similar to that of the VMC. Granitoid plutons from the CFGC at the (sub)surface are highly resistive (Figures 4c and 10a). At deeper midcrustal levels, the highly conductive stack observed below the VMC is extended below the western parts of the GFGC. It is located above a moderately conductive and reflective lower crust that is different from lower crusts in NW sides. Below the CFGC (distances 80–130 km), the lower crust is moderately reflective and conductive, compatible with the presence of the Keitele microcontinent (Lahtinen et al., 2005).

Similarly, in the MT-B2 profile (distances 0–90 km; Figure 10b), the geometry of the VMC is perfectly coherent with the field observation, that is, moderately westward dipping highly to moderately conductive Pirttikylä and Lappfors suites progressively pass to less conductive diatexites and S-type granitoids in the inner part of the VMC. In the SE part of the MT-B2 profile (distances 90–170 km; Figure 10b), supracrustal rocks from the VMC are dipping to the SE and are intruded by granitoids from the CFGC. The hypothetical presence of the Bothnia and Keitele microcontinents is also shown in Figure 10b.

The geometry and the lithological content are similar to that imaged on BABEL 3&4 profile offshore (BABEL working group, 1990) where a stacked accretionary prism above a NE dipping paleosubduction zone was interpreted (BABEL working group, 1990; Korja et al., 1993, 2018). The slab has been interpreted to represent Bothnia microcontinent (Lahtinen et al., 2005). We believe that the VMC could be an onshore prolongation of this accretionary system. In the study area, the Bothnian basin and its basement are stacked against the Keitele orogenic basement underlying the CFGC (Lahtinen et al., 2005; Rämö et al., 2001). The large-scale inverted U-shape crustal conductor (Figure 10b), already reported in other accretionary prisms (e.g., Rao et al., 2007), could be explained by the buttress effect of the rheologically stronger Keitele and Bothnian microcontinent forming the orogenic lower crust during accretion (e.g., Korja et al., 1993). Therefore, we propose that the first-order structures highlighted by the magnetotelluric and seismic profiles represent primary lithological and tectonic features developed during stacking of supracrustal rocks in an accretionary prism (stacks of fertile, wet sediments and large amounts of black shales) and mafic volcanic

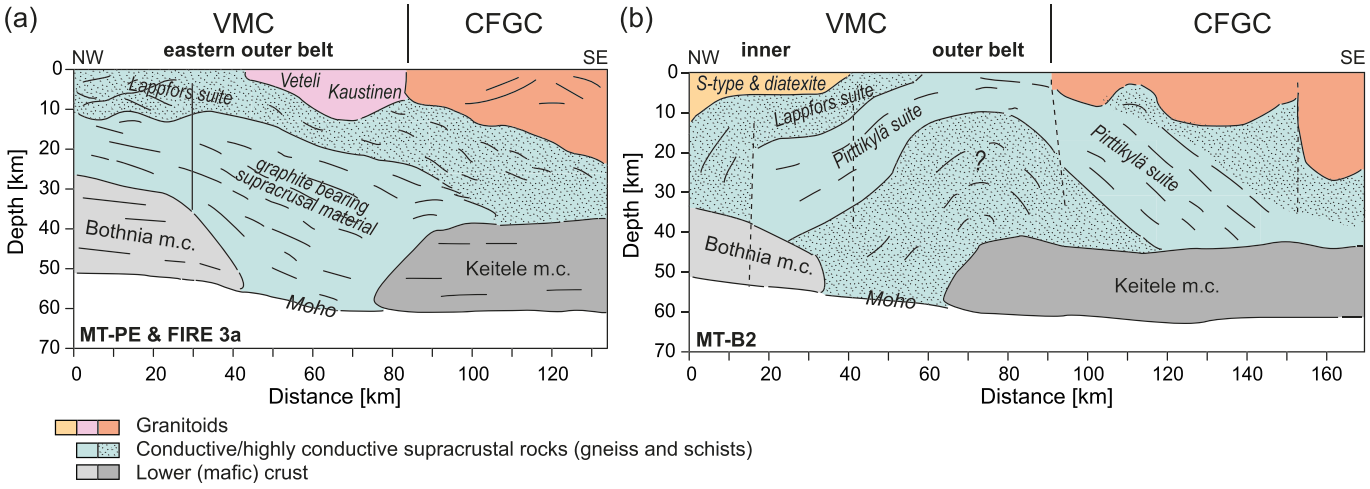

Figure 10. Schematic crustal structure of the VMC and the western part of CFGC based on (a) FIRE 3a profile and MT-PE and (b) MT-B2 models from Figure 4. Locations of the profiles are shown in Figure 2.

slivers (e.g., Lahtinen et al., 2017). Nevertheless, the main structures could have been reactivated, extended, and inverted several times and could have been enhanced by extensional block rotation as proposed by Nikkilä et al. (2016).

6.2. Interpretation of D1 Structural Pattern and Potential Field Data

The first convergent episode D1 (Figure 11a) has developed a dominant S1 N-S striking foliation that is moderately to gently west dipping in most of the VMC. Vaarma and Pipping (1997) have shown that the formation of this metamorphic schistosity is associated with the development of sheath folds and top-to-the E-NE kinematic indicators. The D1 event is connected with moderate crustal thickening that resulted in the development of regional metamorphism ranging from 520–600 °C at 4–5 kbars in the outer part of the complex to 780–875 °C at 5.5–6.5 kbars (i.e., up to the anatexis) in the inner part (Figure 6). The metamorphic zonation and PT estimates reveal an increase in temperature and pressure toward the structurally higher units, that is, from weakly metamorphosed rocks in the east to partially molten rocks in the west. Such an inverted metamorphic zonation is compatible with stacking of the Bothnian basin rocks toward east and formation of a thick accreted sedimentary pile. Overthrusting of hot fold nappe onto less metamorphosed rocks is typically described as a channelized flow of highly ductile material above more rigid rocks (Beaumont et al., 2006). Progressive heating of fertile accretionary wedge may have created a thick migmatite core (Vanderhaeghe , 2009) progressively extruded in the form of a channel flow toward the retrowedge. Such similar early horizontal ductile flow of partially molten middle crust in an accretionary orogen has recently been reported in the Paleozoic CAOB as a major process controlling lateral heat and mass transfer (Jiang et al., 2015; Lehmann et al., 2017).

Moreover, prograde mineral reactions in sulfidic carbon-bearing shales are prone to release abundant fluids by metamorphic devolatilization (H_2O, CO_2, and H_2S) and thus pave the way for large-scale dehydration melting of sedimentary sources (e.g., Ferry, 1981). In the VMC, such lithologies are particularly present in the Pirttikylä suite, and released fluids could have enhanced the anatexis. We can postulate that the presence of graphite schist may influence the thermal gradient within the accretionary prism.

The timing of the primary accretion is framed with U-Pb data throughout the VMC. The oldest metamorphic and magmatic zircon ages at 1.89–1.88 Ga (Kotilainen et al., 2016b; Suikkanen et al., 2014, and references therein) correspond to the onset of partial melting of the thickened stack of accretionary wedge sediments (Figure 11a). The metamorphic peak in the evolution of the VMC was probably reached at around 1.87 Ga, as shown by the widespread presence of in situ S-type granitoid at this time. The roughly westward accretion (D1) of the Bothian basin rocks toward Karelian continent is coeval with intense I-type, primitive to normal, calc-alkaline arc magmatism in the CFGC at 1.89–1.88 Ga resulting from the partial melting of accreted mafic to intermediate lower to middle crust (Nikkilä et al., 2016). The age of magmatism and the

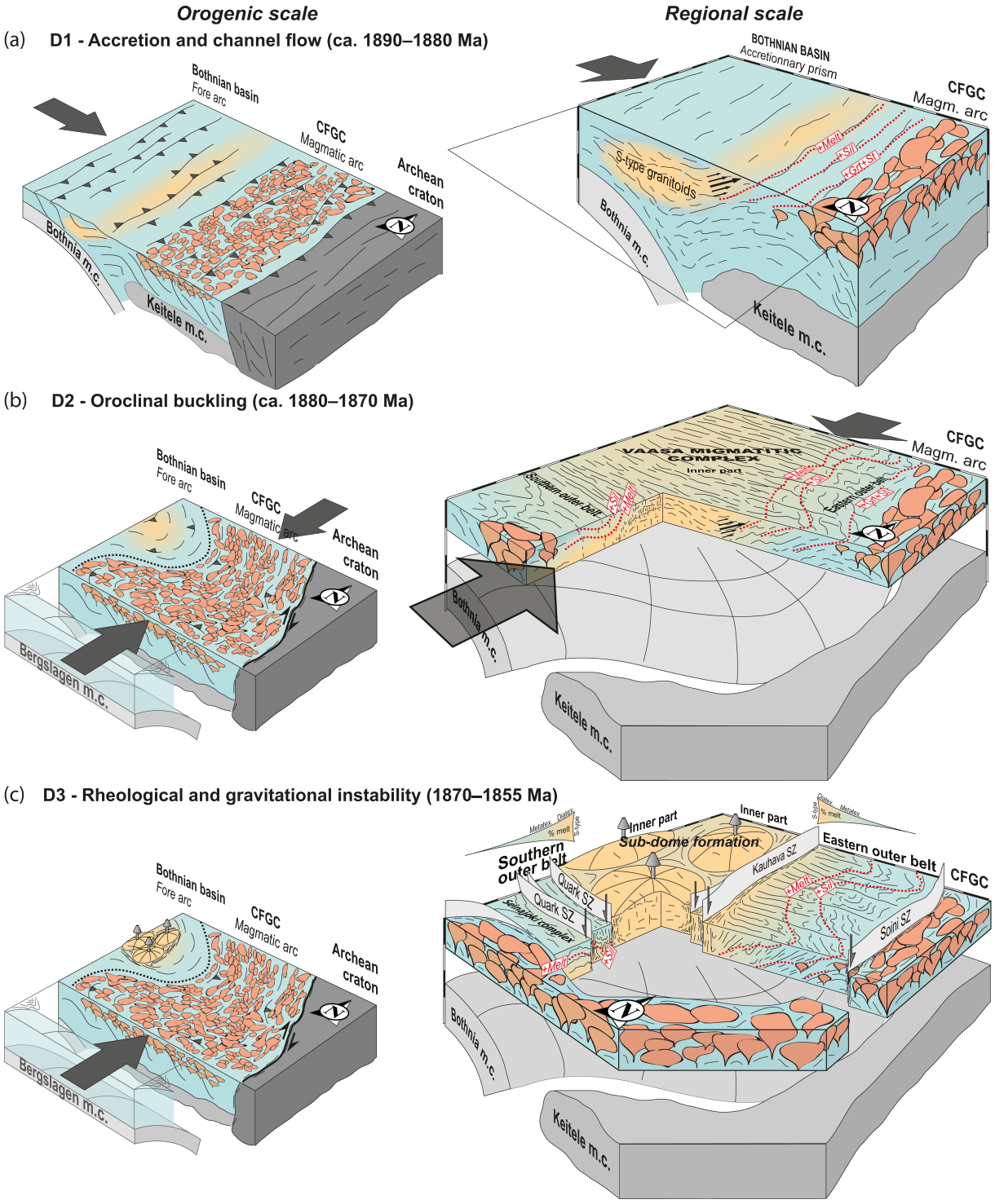

Figure 11. An idealized tectonic model for the VMC from the basin accretion and partial melting (D1, a), to buckling (D2, b), and to vertical transfer (D3, c).

first occurrence of S-type magmatism and metamorphism in the VMC support the idea that 1.89 Ga is the minimum age for the arc formation and the contemporaneous basin accretion and the associated anatexis (Lahtinen et al., 2005; Nikkilä et al., 2016; Sorjonen-Ward, 2006).

The D1 accretion has also been described from the Pirkanmaa-Tampere belt south of the CFGC (Lahtinen et al., 2009) and from the Robertsfors complex south of the Skellefte belt in Sweden (Skiöld & Rutland,

2006). Based on the major continuous conductor anomaly (Figure 1b), Gorbatschev and Bogdanova (1993) and later Lahtinen et al. (2014, 2017) proposed that the prisms have initially been part of the same linear accretionary system until 1.87 Ga.

6.3. Significance of D2 Orthogonal Shortening (Oroclinal Buckling)

A major tectonic shift is observed after the development of the primary orogenic fabric. We observe a roughly N-S D2 regional shortening (Figure 11b) responsible for the heterogeneous development of E-W upright folds and associated S2 subvertical axial planar schistosity, crosscutting the early metamorphic zoning. In the mica schists, only open F2 folds are observed, whereas close to isoclinal F2 folds are widespread in metatexites. We propose that this reflects different rheological behavior of the metasediments with respect to the metatexites, as increasing amount of melt reduces competence (e.g., Vanderhaeghe, 2009). In the metatexites, the axial planar cleavage S2 may either collect granitic melt (Figure 7g) or it may be developed within andalusite stability field because cordierite is breaking down to And + Bt (Figures 9d and 9e). The development is compatible with a retrograde evolution during D2, from temperature above the melt-in line (>675 °C; Figure 9b) toward lower temperatures of 550 °C. Macroscopic E-W trending vertical magmatic foliation has been observed in the inner part of the VMC (Sipilä et al., 2008), suggesting N-S shortening during the emplacement and/or cooling of the S-type granitoids.

The D2 major N-S regional shortening observed in the VMC has also been described in other parts of the Svecofennian orogen. In the CFGC, it developed conjugate NW-SE striking dextral ductile shear zones and roughly E-W striking magmatic to subsolidus planar fabrics (Nikkilä et al., 2016; Nironen, 2003; Nironen et al., 2000). The shear zones are interpreted to have been active in the CFGC at around 1.88 Ga or later (Nikkilä et al., 2016; Nironen et al., 2000) and the E-W striking metamorphic fabrics a few million years before (Nikkilä et al., 2016). In the Tampere-Pirkanmaa belts, the D2 deformation has produced upright tight to isoclinal F2 E-W striking folds and associated axial planar S2 schistosity (Kilpeläinen, 1998; Nironen, 1989). To the north, orthogonal deformation successions is also observed in the Martimo belt (Lahtinen et al., 2015). In the Robertsfors complex, similar vertical D2 structures striking ENE-WSW (Rutland et al., 2001; Skiöld & Rutland, 2006) are probably younger than 1.88 Ga. This indicates that the D2 N-S shortening is not a local tectonic event but is the main tectonic event controlling the geometry of the entire central Svecofennian orogen (Figure 11b).

Recently, Lahtinen et al. (2014, 2017) proposed that the folded architecture of the conductor anomaly in the map view results from the buckling of the linear accretionary system from 1.87 to 1.86 Ga due to dextral transpression along the Karelian continental margin. Our data are fully compatible with this model (Figure 11b), where the regional N-S shortening (D2) marks the start of the orogenic buckling and the southward migration of the accretionary system (Bogdanova et al., 2015). Another accretionary model by Nironen (2017) implies several subduction zones, accretionary prisms, and microcontinents. He explains the formation of the VMC at the margin of the Keitele microcontinent (i.e., the mafic granulitic lower crust beneath the CFGC) by northward migration of the Bothnian and Bergslagen microcontinents at 1.90–1.87 Ga. This could also correspond to our D2 tectonic event. Nevertheless, it does not explain the early anatexis of the supracrustal rocks in a different accretionary setting (D1). Consequently, we suggest here that D2 is an orogenic-scale event, reflecting switch from E-W channel flow dynamics to major N-S shortening. The structural template described here is consistent with the formation of giant crustal fold affecting the length of the accretionary prism. On a larger scale, the folding is imaged by the bending of conductive supracrustal rocks (Korja et al., 2002) in the form of an orocline (Lahtinen et al., 2014, 2017). The northward movement of the Bergslagen microcontinent toward the already accreted Bothnian and Keitele could result in the formation of the orocline and contemporaneous dextral transpression along the Karelian margin (Figure 11b).

6.4. Significance of D3 Vertical Flow (Late Gravity Overturns in the Hinge Zone of an Orocline)

The last major tectonic event is represented by D3 vertical shearing mainly at the boundaries between the inner and outer parts of the VMC (Kauhava and Quark shear zones) and within the diatexites separating subrounded granitoids within the inner part of the VMC (Figure 11c). The buoyancy contrast between unmolten and molten rocks together with loss of continuity of the solid framework, that is, from metatexites to diatexites and granites (e.g., Vanderhaeghe, 2009), may have provoked buoyancy-dominated flow in the VMC inner part (Figures 3b and 11c). This could have induced diapirism of less dense and viscous

material expressed as the formation of granitoid subdomes surrounded by diatexites (e.g., Kruckenberg et al., 2011; Rey et al., 2011; Vanderhaeghe et al., 2018). At a regional scale, vertical transfer of molten middle crust has been localized in the hinge core of the orocline (Figure 11c). We suggest that the formation of a moderately plunging oroclinal hinge filled with low density and viscosity partially molten rocks and granitoids has opened pathways for the magmatic zone at the late stage of (or post) of D2 in N-S regional shortening. Finally, the magma may locally have become diapiric thus separating the downward pointing cusps of diatexites from the local subdomes. On a large scale, the steep Kauhava and Quark shear zones separated the less molten parts of metamorphic envelope from subdomes formed by partially molten vertically flowing core. Widespread magmatic activity, including crust-derived felsic magma, is also reported in other similar systems such as the Cantabrian oroclines in the European Variscan belt where post accretionary buckling and subsequent collision is associated with a high thermal anomaly (Weil et al., 2019).

The timing of D3 in the VMC can be approximated with the published zircon and monazite age data. The youngest magmatic zircons from the inner part of VMC are approximately 1,865 Myr old (Kotilainen et al., 2016b; Suikkanen et al., 2014). The ages are contemporaneous with the cluster of available monazite ages from mica schists and migmatites (ca. 1,864 Ma; Alviola et al., 2001; Sipilä et al., 2008; Kotilainen et al., 2016a). This may represent the age of last magmatic pulses together with the general cooling of the complex during its extrusion, the monazite ages representing the (re)crystallization in the amphibolite facies at around 550 °C and 3–4 kbars (Figure 9b). The extracted magma could have kept the surrounding rocks at higher temperatures (Williams & Karlstrom, 1996), thus slowing the cooling and provoking a weak decrease of the zircon and monazite ages away from the VMC inner part (Kotilainen et al., 2016a, 2016b). Several papers point out the importance of late orogenic extension and lateral spreading following accretionary processes in particular within the nearby CFGC (e.g., Korja et al., 2009; Nikkilä et al., 2015). There, NE-SW to N-S striking moderately dipping to low angle normal faults (Nironen, 2003) can be traced at crustal scale in seismic profiles (Korja et al., 2009). These kinds of faults have not been detected in our field area, in particular, between the inner and the outer VMC or between the CFGC and the VMC. Indeed, we have observed only subvertical (ductile) shear zones with vertical movement, and not late vertical shortening have been detected. Therefore, a classic (extensional) metamorphic core complex tectonic model cannot explain the present general structure of the VMC. However, numerical modeling show that extension in the upper crust can enhance convergent migmatitic flow and development of "double domes" separated by high-strain vertical deformation zone (Rey et al., 2011) such as observed in the VMC inner part. Moreover, the vertical boundary between VMC and CFGC (Soini shear zone) could result from the steepening of an originally low angle fault (Nikkilä et al., 2016).

6.5. Early Accretionary System Along the Columbia/Nuna Supercontinent

The Svecofennian orogen is part of a long lasting (1.90–1.30 Ga) accretionary orogen formed along the newly assembled (2.10−1.80 Ga) Columbia/Nuna supercontinent (Meert, 2012; Rogers & Santosh, 2002; Zhao et al., 2002, 2004). Together with the Penokean orogen in North America (Schulz & Cannon, 2007), the Svecofennian orogen represents the early relics of this accretionary system responsible for a massive crustal growth during the Paleo-Mesoproterozoic. Accretionary orogens are formed by the continuous accretion of arc, basins, island arc, and oceanic plateau along a stable continent (e.g., Cawood et al., 2009). By Collins (2002a, 2002b) and Collins and Richards (2008), the typical LP-HT regional metamorphism affecting the supracrustal rocks up to the anatexis in accretionary orogens is explained by the advective mantle heat affecting back-arc basins. In the model, the peak of metamorphism takes place in extensional setting before convergent accretion due to tectonic switching. In our study, the primary source of the Bothnian basin, the protolith of the VMC, is the nearby Karelian continental margin, with only few arc-related sediments (Claesson et al., 1993; Kotilainen et al., 2016b; Lahtinen et al., 2002; Lahtinen et al., 2016), and the peak metamorphism is developed during D1, that is, convergent accretionary phase. Therefore, we propose that the LP-HT metamorphism in the VMC results from (1) the retreat of the subducting slab provoking a local heating of the Bothnian basin and (2) its subsequent accretion (D1) developing the regional metamorphism, associated anatexis and channel flow. The VMC could have registered an earlier tectonic switch than the one suggested for the western Svecofennian orogen in Sweden (Hermansson et al., 2008). The subsequent N-S regional shortening (D2) and associated orogenic buckling in the Svecofennian orogen at ca. 1.87 Ga might reflect a larger-scale plate tectonic reorganization such as the beginning of the collision of Baltica and Volgo-Sarmatia (Bogdanova et al., 2015; Johansson, 2009; Lahtinen et al., 2005).

7. Conclusions

The geophysical, structural, metamorphic, and geochronological data deliver a comprehensive model for the origin and evolution of a major Precambrian crust-derived magmatic body.

1. The VMC records D1 prograde metamorphism ranging from 520 to 850 °C and from 4 to 6.5 kbars from the outer part to the inner part, respectively. This metamorphism resulted from the (northward) westward accretion of the supracrustals rocks, with a thermal maturation reaching anatexis at 1.89–1.88 Ga and peaking at ca. 1.87 Ga. It is in line with the development of a channel flow permitting gradual juxtaposition of metamorphosed and partially molten supracrustal rocks and creating an inverted gradient.
2. Subsequent N-S D2 shortening at 1.87 Ga formed E-W striking folds and S2 subvertical axial planar schistosity in the outer part of the VMC, whereas D3 buoyancy-driven gravitational instabilities and the rise of subdomes are observed in the inner part. This type of magmatic extraction might have intensified the HT-LP metamorphism in the surrounding rocks. D3 vertical shearing at the border of the VMC, at the limit between its inner and outer parts and between the subdomes, enhanced vertical exchanges and cooling of the VMC up to andalusite stability field (550 °C and 3–4 kbars) at about ca. 1,865 Ma.
3. The D1 accretion in the VMC is coeval with the formation of the eastern CFGC at 1.89 Ga and contemporaneous with the formation of similar supracrustal belts of the Svecofennian orogen. Regional D2 shortening in the VMC supports the idea of an orogenic northward convergence of the Bergslagen microcontinent starting no later than 1.87 Ga and provoking the buckling of the supracrustal belt and the transpression along the Karelian continental margin.
4. Seismic and MT profiles highlight primary stacking structures such as the geometry of an accretionary wedge affected by channel flow of stacked supracrustal rocks (VMC) upon rigid promontory (Bothnian and Keitele microcontinents).
5. The beginning of the accretion and the associated prograde metamorphism at ca. 1.90 Ga ago might be part of the first recorded tectonic switch in the Svecofennian orogen along the Columbia/Nuna supercontinent.

Acknowledgments
This work has been supported by the Academy of Finland through the MIDCRUST consortium 139035, 139549, and 139516. We thank the University of Oulu for the researcher exchange grants to M. A. Zaher. We also acknowledge the grants from the K.H. Renlund's Foundation to MIDCUST consortium. We thank the IPGS UMR 7516 for its financial support. We are grateful to Olivier Vanderhaeghe and Fawna Korhonen for detailed constructive reviews. Ernst Willingshofer is thanked for his comments and editorial work. FIRE data are published in OpenFIRE application (https://avaa.tdata.fi/web/fire), and Broadband magnetotelluric data (MT-PE and MT-B2) are available in the EPOS-ERIC Thematic core service repository (http://ics-c.epos-ip.org/data/search).

References

Alviola, R., Mänttäri, I., Mäkitie, H., & Vaasjoki, M. (2001). Svecofennian rare-element granitic pegmatites of the Ostrobothnia region, western Finland; their metamorphic environment and time of intrusion. In H. Mäkitie (Ed.), *Svecofennian granitic pegmatites (1.86-1.79 Ga) and quartz monzonite (1.87 Ga), and their metamorphic environment in the Seinäjoki region, western Finland*, *Geological Survey of Finland, Special Paper* (Vol. 30, pp. 9–29). Finland, Espoo: Geological Survey of Finland.

BABEL working group (1990). Evidence for early Proterozoic plate tectonics from seismic reflection profiles in the Baltic shield. *Nature*, *348*(6296), 34–38. https://doi.org/10.1038/348034a0

Beaumont, C., Nguyen, M., Jamieson, R. A., & Ellis, S. (2006). Crustal flow modes in large hot orogens. *Geological Society, London, Special Publications*, *218*, 91–145. https://doi.org/10.1144/GSL.SP.2006.268.01.05

Berthé, D., Choukroune, P., & Jegouzo, P. (1979). Orthogneiss, mylonite and no-coaxial deformation of granites: The example from the South Armorican Shear Zone. *Journal of Structural Geology*, *1*, 31–42. https://doi.org/10.1016/0191-8141(79)90019-1

Bogdanova, S., Gorbatschev, R., Skridlaite, G., Soesoo, A., Taran, L., & Kurlovich, D. (2015). Trans-Baltic Palaeoproterozoic correlations towards the reconstruction of supercontinent Columbia/Nuna. *Precambrian Research*, *259*, 5–33. https://doi.org/10.1016/j.precamres.2014.11.023

Cagnard, F., Durrieu, N., Gapais, D., Brun, J.-P., & Ehlers, C. (2006). Crustal thickening and lateral flow during compression of hot lithospheres, with particular reference to Precambrian times. *Terra Nova*, *18*(1), 72–78. https://doi.org/10.1111/j.1365-3121.2005.00665.x

Cagnard, F., Gapais, D., & Barbey, P. (2007). Collision tectonics involving juvenile crust: The example of the southern Finnish Svecofennides. *Precambrian Research*, *154*(1), 125–141. https://doi.org/10.1016/j.precamres.2006.12.011

Cawood, P. A., Kröner, A., Collins, W. J., Kusky, T. M., Mooney, W. D., & Windley, B. F. (2009). Accretionary orogens through Earth history. *Geological Society, London, Special Publications*, *318*(1), 1–36. https://doi.org/10.1144/sp318.1

Chardon, D., Gapais, D., & Cagnard, F. (2009). Flow of ultra-hot orogens: A view from the Precambrian, clues for the Phanerozoic. *Tectonophysics*, *477*(3–4), 105–118. https://doi.org/10.1016/j.tecto.2009.03.008

Claesson, S., Huhma, H., Kinny, P. D., & Williams, I. S. (1993). Svecofennian detrital zircon ages—Implications for the Precambrian evolution of the Baltic Shield. *Precambrian Research*, *64*(1), 109–130. https://doi.org/10.1016/0301-9268(93)90071-9

Collins, W. J. (2002a). Hot orogens, tectonic switching, and creation of continental crust. *Geology*, *30*(6), 535–538. https://doi.org/10.1130/0091-7613(2002)030<0535:HOTSAC>2.0.CO;2

Collins, W. J. (2002b). Nature of extensional accretionary orogens. *Tectonics*, *21*(4), 1024. https://doi.org/10.1029/2000TC001272

Collins, W. J., & Richards, S. W. (2008). Geodynamic significance of S-type granites in circum-Pacific orogens. *Geology*, *36*(7), 559–562. https://doi.org/10.1130/G24658A.1

Cosgrove, J. W. (1997). The influence of mechanical anisotropy on the behaviour of the lower crust. *Tectonophysics*, *280*(1–2), 1–14. https://doi.org/10.1016/S0040-1951(97)00145-5

Costa, S., & Rey, P. (1995). Lower crustal rejuvenation and growth during post-thickening collapse: Insights from a crustal cross section through a Variscan metamorphic core complex. *Geology*, *23*, 10, 905–10,908. https://doi.org/10.1130/0091-7613(1995)023<0905:LCRAGD>2.3.CO;2

Culshaw, N. G., Beaumont, C., & Jamieson, R. A. (2006). The orogenic superstructure-infrastructure concept: Revisited, quantified, and revived. *Geology*, *34*(9), 733–736. https://doi.org/10.1130/g22793.1

Dewey, J. F. (1988). Extensional collapse of orogens. *Tectonics*, *7*(6), 1123–1139. https://doi.org/10.1029/TC007i006p01123
Ferry, J. M. (1981). Petrology of graphitic sulfide-rich schists from South-central Maine: An example of desulfidation during prograde regional metamorphism. *American Mineralogist*, *66*(9–10), 908–930.
Foster, D. A., & Gray, D. R. (2000). Evolution and structure of the Lachlan Fold Belt (Orogen) of Eastern Australia. *Annual Review of Earth and Planetary Sciences*, *28*(1), 47–80. https://doi.org/10.1146/annurev.earth.28.1.47
Gaál, G., & Gorbatschev, R. (1987). An outline of the Precambrian evolution of the Baltic shield. *Precambrian Research*, *35*, 15–52. https://doi.org/10.1016/0301-9268(87)90044-1
Gapais, D., Jaguin, J., Cagnard, F., & Boulvais, P. (2014). Pop-down tectonics, fluid channelling and ore deposits within ancient hot orogens. *Tectonophysics*, *618*, 102–106. https://doi.org/10.1016/j.tecto.2014.01.027
Geological Survey of Finland (2012). DigiKP200 - 1:200 000 bedrock map of Finland, Geological Survey of Finland. https://gtkdata.gtk.fi/Kalliopera/index.html [accessed 28/01/2020].
Glen, R. A., Korsch, R. J., Direen, N. G., Jones, L. E. A., Johnstone, D. W., Lawrie, K. C., et al. (2002). Crustal structure of the Ordovician Macquarie Arc, Eastern Lachlan Orogen, based on seismic-reflection profiling. *Australian Journal of Earth Sciences*, *49*(2), 323–348. https://doi.org/10.1046/j.1440-0952.2002.00925.x
Gorbatschev, R., & Bogdanova, S. (1993). Frontiers in the Baltic shield. *Precambrian Research*, *64*(1), 3–21. https://doi.org/10.1016/0301-9268(93)90066-B
Grad, M., Tiira, T., & Group WESC (2009). The Moho depth map of the European Plate. *Geophysical Journal International*, *176*(1), 279–292. https://doi.org/10.1111/j.1365-246X.2008.03919.x
Guy, A., Schulmann, K., Janoušek, V., Štípská, P., Armstrong, R., Belousova, E., et al. (2015). Geophysical and geochemical nature of relaminated arc-derived lower crust underneath oceanic domain in southern Mongolia. *Tectonics*, *34*, 1030–1053. https://doi.org/10.1002/2015TC003845
Guy, A., Schulmann, K., Munschy, M., Miehe, J. M., Edel, J.-B., Lexa, O., & Fairhead, D. (2014). Geophysical constraints for terrane boundaries in southern Mongolia. *Journal of Geophysical Research: Solid Earth*, *119*(10), 7966–7991. https://doi.org/10.1002/2014JB011026
Hermansson, T., Stephens, M. B., Corfu, F., Page, L. M., & Andersson, J. (2008). Migratory tectonic switching, western Svecofennian orogen, central Sweden: Constraints from U/Pb zircon and titanite geochronology. *Precambrian Research*, *161*(3), 250–278. https://doi.org/10.1016/j.precamres.2007.08.008
Hölttä, P., & Heilimo, E. (2017). Metamorphic map of Finland. In M. Nironen (Ed.), *Bedrock of Finland at the scale 1:1 000 000—Major stratigraphic units, metamorphism and tectonic evolution*, *Geological Survey of Finland, Special Paper* (Vol. 60, pp. 77–128). Finland, Espoo: Geological Survey of Finland.
Jiang, Y. D., Štípská, P., Sun, M., Schulmann, K., Zhang, J., Wu, Q. H., et al. (2015). Juxtaposition of Barrovian and migmatite domains in the Chinese Altai: A result of crustal thickening followed by doming of partially molten lower crust. *Journal of Metamorphic Geology*, *33*(1), 45–70. https://doi.org/10.1111/jmg.12110
Johansson, Å. (2009). Baltica, Amazonia and the SAMBA connection—1000 million years of neighbourhood during the Proterozoic? *Precambrian Research*, *175*(1), 221–234. https://doi.org/10.1016/j.precamres.2009.09.011
Kähkönen, Y. (2005). Chapter 8 Svecofennian supracrustal rocks. *Developments in Precambrian Geology*, *14*, 343–405. https://doi.org/10.1016/S0166-2635(05)80009-X
Karlstrom, K. E., & Williams, M. L. (1998). Heterogeneity of the middle crust: Implications for strength of continental lithosphere. *Geology*, *26*(9), 815–818. https://doi.org/10.1130/0091-7613(1998)026<0815:HOTMCI>2.3.CO;2
Kidan, T. W., & Cosgrove, J. W. (1996). The deformation of multilayers by layer-normal compression; an experimental investigation. *Journal of Structural Geology*, *18*(4), 461–474. https://doi.org/10.1016/0191-8141(95)00099-Y
Kilpeläinen, T. (1998). *Evolution and 3D modelling of structural and metamorphic patterns of the Palaeoproterozoic crust in the Tampere-Vammala area, southern Finland*, Geological Survey of Finland Bulletin (Vol. 397, p. 124). Espoo: Geological Survey of Finland.
Koistinen, T., Stephens, M. B., Bogatchev, V., Nordgulen, Ø., Wennerström, M., & Korhonen, J. (2001). Geological map of the Fennoscandian Shield, scale 1:2,000,000. Espoo: Geological Survey of Finland, Trondheim: Geological Survey of Norway, Uppsala: Geological Survey of Sweden, Moscow: Ministry of Natural Resources of Russia.
Korhonen, J. V. (2005). Airborne magnetic method: Special features and review on applications. In M.-L. Airo (Ed.), *Aerogeophysics in Finland 1972–2004: Methods, system characteristics and applications*, *Geological Survey of Finland, Special Paper* (Vol. 39, pp. 77–102). Espoo: Geological Survey of Finland.
Korhonen, J. V., Aaro, S., All, T., Elo, S., Haller, L. A., Kääriäinen, J., et al. (2002). Bouguer anomaly map of the Fennoscandian Shield 1:2000000, Geological Surveys of Finland, Norway and Sweden and Ministry of Natural Resources of Russian Federation.
Korhonen, J. V., Aaro, S., All, T., Nevanlinna, H., Skilbrei, J. R., Säävuori, H., et al. (2002). Magnetic anomaly map of the Fennoscandian Shield 1:2000000, Geological Surveys of Finland, Norway and Sweden and Ministry of Natural Resources of Russian Federation.
Korja, A., & Heikkinen, P. (2005). The accretionary Svecofennian orogen—Insight from the BABEL profiles. *Precambrian Research*, *136*(3), 241–268. https://doi.org/10.1016/j.precamres.2004.10.007
Korja, A., Heikkinen, P., Tiira, P., & Nikkilä, K. (2018). BABEL3&3a: Crustal-scale structures of the Precambrian Svecofennian accretionary orogen in the Fennoscandian Shield. In A. A. Misra & S. Mukherjee (Eds.), *Atlas of Structural Geological Interpretation from Seismic Images* (pp. 205–208). Hoboken, NJ: John Wiley & Sons Ltd. https://doi.org/10.1002/9781119158332.ch40
Korja, A., & Heikkinen, P. J. (2008). Seismic images of Paleoproterozoic microplate boundaries in the Fennoscandian Shield. In K. C. Condie & V. Pease (Eds.), *When did plate tectonics begin on planet Earth? Geological Society of America Special Paper* (Vol. 440, pp. 229–248). Boulder, CO: Geological Society of America.
Korja, A., Korja, T., Luosto, U., & Heikkinen, P. (1993). Seismic and geoelectric evidence for collisional and extensional events in the Fennoscandian Shield implications for Precambrian crustal evolution. *Tectonophysics*, *219*(1), 129–152. https://doi.org/10.1016/0040-1951(93)90292-R
Korja, A., Kosunen, P., & Heikkinen, P. (2009). A case study of lateral spreading: The Precambrian Svecofennian Orogen. *Geological Society, London, Special Publications*, *321*(1), 225–251. https://doi.org/10.1144/sp321.11
Korja, A., Lahtinen, R., & Nironen, M. (2006). The Svecofennian orogen: A collage of microcontinents and island arcs. *Geological Society, London, Memoirs*, *32*(1), 561–578. https://doi.org/10.1144/gsl.mem.2006.032.01.34
Korja, T., Engels, M., Zhamaletdinov, A. A., Kovtun, A. A., Palshin, N. A., Smirnov, M. Y., et al. (2002). Crustal conductivity in Fennoscandia—A compilation of a database on crustal conductance in the Fennoscandian Shield. *Earth, Planets and Space*, *54*(5), 535–558. https://doi.org/10.1186/bf03353044

Korja, T., & Hjelt, S. E. (1993). Electromagnetic studies in the Fennoscandian Shield—Electrical conductivity of Precambrian crust. *Physics of the Earth and Planetary Interiors*, *81*(1), 107–138. https://doi.org/10.1016/0031-9201(93)90127-U

Korja, T., Vaittinen, K., Zaher, M. A., Pirttijärvi, M., Lahti, I., Smirnov, M., & Kaikkonen, P. (2013). Crustal conductivity in the Bothnian region (Oulu-Vaasa): Implications for crustal structure and evolution. In T. Veikkolainen, K. Suhonen, J. Näränen, T. Korja, K. Kauristie, & S. Kaasalainen (Eds.), *XXVI Geofysiikan Päivät* (pp. 55–58). Helsinki: Geophysical Society of Finland.

Korsman, K., Koistinen, T., Kohonen, J., Wennerström, M., Ekdahl, E., Honkamo, M., et al. (1997). *Suomen kallioperäkartta – Berggrundskarta över Finland – Bedrock map of Finland 1: 1 000 000*. Espoo, Finland: Geological Survey of Finland.

Korsman, K., Korja, T., Pajunen, M., Virransalo, P., & GGT/SVEKA Working Group (1999). The GGT/SVEKA Transect: Structure and evolution of the continental crust in the Paleoproterozoic Svecofennian orogen in Finland. *International Geology Review*, *41*(4), 287–333. https://doi.org/10.1080/00206819909465144

Kotilainen, A. K., Mänttäri, I., Kurhila, M., Hölttä, P., & Rämö, O. T. (2016a). New monazite U-Pb constraints on the evolution of the Paleoproterozoic Vaasa granitoid batholith, western Finland. *Bulletin of the Geological Society of Finland*, *88*(1–2), 5–20. https://doi.org/10.17741/bgsf/88.1.001

Kotilainen, A. K., Mänttäri, I., Kurhila, M., Hölttä, P., & Rämö, O. T. (2016b). Evolution of a Palaeoproterozoic giant magmatic dome in the Finnish Svecofennian; New insights from U–Pb geochronology. *Precambrian Research*, *272*, 39–56. https://doi.org/10.1016/j.precamres.2015.10.023

Kousa, J., & Lundqvist, T. (2000). Svecofennian Domain. In T. Lundqvist & S. Autio (Eds.), *Description to the bedrock map of Central Fennoscandia (Mid-Norden)*, *Geological Survey of Finland, Special Paper* (Vol. 28, pp. 47–75). Espoo, Finland: Geological Survey of Finland.

Kruckenberg, S. C., Vanderhaeghe, O., Ferré, E. C., Teyssier, C., Whitney, D. L., & Chapman, A. (2011). Flow of partially molten crust and the internal dynamics of a migmatite dome, Naxos, Greece. *Tectonics*, *30*, TC3001. https://doi.org/10.1029/2010TC002751

Kukkonen, I. T., Heikkinen, P., Ekdahl, E., Hjelt, S., Yliniemi, J., Jalkanen, E., & FIRE Working Group (2006). Acquisition and geophysical characteristics of reflection seismic data on FIRE transects, Fennoscandian Shield. In I. T. Kukkonen & R. Lahtinen (Eds.), *Finnish Reflection Experiment FIRE 2001–2005*, Geological Survey of Finland, *Special Paper* (Vol. 43, pp. 13–43). Espoo: Geological Survey of Finland.

Lahtinen, R., Huhma, H., & Kousa, J. (2002). Contrasting source components of the Paleoproterozoic Svecofennian metasediments: Detrital zircon U–Pb, Sm–Nd and geochemical data. *Precambrian Research*, *116*(1), 81–109. https://doi.org/10.1016/S0301-9268(02)00018-9

Lahtinen, R., Huhma, H., Lahaye, Y., Lode, S., Heinonen, S., Sayab, M., & Whitehouse, M. J. (2016). Paleoproterozoic magmatism across the Archean-Proterozoic boundary in central Fennoscandia: Geochronology, geochemistry and isotopic data (Sm–Nd, Lu–Hf, O). *Lithos*, *262*, 507–525. https://doi.org/10.1016/j.lithos.2016.07.014

Lahtinen, R., Huhma, H., Sipilä, P., & Vaarma, M. (2017). Geochemistry, U-Pb geochronology and Sm-Nd data from the Paleoproterozoic Western Finland supersuite—A key component in the coupled Bothnian oroclines. *Precambrian Research*, *299*, 264–281. https://doi.org/10.1016/j.precamres.2017.07.025

Lahtinen, R., Johnston, S. T., & Nironen, M. (2014). The Bothnian coupled oroclines of the Svecofennian Orogen: A Palaeoproterozoic terrane wreck. *Terra Nova*, *26*(4), 330–335. https://doi.org/10.1111/ter.12107

Lahtinen, R., Korja, A., & Nironen, M. (2005). Paleoproterozoic tectonic evolution. *Developments in Precambrian Geology*, *14*, 481–531. https://doi.org/10.1016/S0166-2635(05)80012-X

Lahtinen, R., Korja, A., Nironen, M., & Heikkinen, P. (2009). Palaeoproterozoic accretionary processes in Fennoscandia. *Geological Society, London, Special Publications*, *318*(1), 237–256. https://doi.org/10.1144/sp318.8

Lahtinen, R., Sayab, M., & Fredrik, K. (2015). Near-orthogonal deformation successions in the poly-deformed Paleoproterozoic Martimo belt: Implications for the tectonic evolution of Northern Fennoscandia. *Precambrian Research*, *270*, 22–38. https://doi.org/10.1016/j.precamres.2015.09.003

Lehmann, J., Schulmann, K., Lexa, O., Závada, P., Štípská, P., Hasalová, P., et al. (2017). Detachment folding of partially molten crust in accretionary orogens: A new magma-enhanced vertical mass and heat transfer mechanism. *Lithosphere*, *9*(6), 889–909. https://doi.org/10.1130/L670.1

Lehtonen, M. I., Kujala, H., Kärkkäinen, N., Lehtonen, A., Mäkitie, H., Mänttäri, I., et al. (2003). *Etelä-Pohjanmaan liuskealueen kallioperä. Summary: Pre-Quaternary rocks of the South Ostrobothnian Schist Belt*, Report of Investigation (Vol. *158*, p. 125). Espoo: Geological Survey of Finland.

Leväniemi, H., Beamish, D., Hautaniemi, H., Kurimo, M., Suppala, I., Vironmäki, J., et al. (2009). The JAC airborne EM system: AEM-05. *Journal of Applied Geophysics*, *67*(3), 219–233. https://doi.org/10.1016/j.jappgeo.2007.10.001

Lundqvist, T., Bøe, R., Kousa, J., Lukkarinen, H., Lutro, O., Roberts, D., et al.. (1996). Bedrock map of central Fennoscandia. Scale 1:1 000 000, Geological Surveys of Finland (Espoo), Norway (Trondheim) and Sweden (Uppsala).

Luukas, J., Kousa, J., Nironen, M., & Vuollo, J. (2017). Major stratigraphic units in the bedrock of Finland, and an approach to tectonostratigraphic division. In M. Nironen (Ed.), *Bedrock of Finland at the scale 1:1 000 000 - Major stratigraphic units, metamorphism and tectonic evolution*, *Special Paper* (Vol. 60, pp. 9–40). Finland: Geological Survey.

Mäkitie, H. (2001). Eastern margin of the Vaasa Migmatite Complex, Kauhava, western Finland: preliminary petrography and geochemistry of the diatexites. *Bulletin of the Geological Society of Finland*, *73*, 35–46.

Mäkitie, H., Kärkkäinen, N., Lahti, S. I., & Alviola, R. (2001). Compositional variation of granitic pegmatites in relation to regional metamorphism in the Seinäjoki region, western Finland. In H. Mäkitie (Ed.), *Svecofennian granitic pegmatites (1.86-1.79 Ga) and quartz monzonite (1.87 Ga), and their metamorphic environment in the Seinäjoki region, western Finland*, *Special Paper* (Vol. 30, pp. 31–59). Espoo: Geological Survey of Finland.

Mäkitie, H., & Lahti, S. I. (2001). The fayalite-augite quartz monzonite (1.87 Ga) of Luopa, western Finland, and its contact aureole. In H. Mäkitie (Ed.), *Svecofennian granitic pegmatites (1.86-1.79 Ga) and quartz monzonite (1.87 Ga), and their metamorphic environment in the Seinajoki region, western Finland*, *Special Paper* (Vol. 30, pp. 61–98). Espoo: Geological Survey of Finland.

Mäkitie, H., Sipilä, P., Kujala, H., Lindberg, A., & Kotilainen, A. (2012). Formation of the Vaasa batholith in the Fennoscandian shield: Petrographic and geochemical constraints. *Bulletin of the Geological Society of Finland*, *84*, 141–166.

Meert, J. G. (2012). What's in a name? The Columbia (Paleopangaea/Nuna) supercontinent. *Gondwana Research*, *21*(4), 987–993. https://doi.org/10.1016/j.gr.2011.12.002

Nikkilä, K., Korja, A., Koyi, H., & Eklund, O. (2015). Analog modeling of one-way gravitational spreading of hot orogens—A case study from the Svecofennian orogen, Fennoscandian Shield. *Precambrian Research*, *268*, 135–152. https://doi.org/10.1016/j.precamres.2015.07.011

Nikkilä, K., Mänttäri, I., Nironen, M., Eklund, O., & Korja, A. (2016). Three stages to form a large batholith after terrane accretion—An example from the Svecofennian orogen. *Precambrian Research*, *281*, 618–638. https://doi.org/10.1016/j.precamres.2016.06.018

Nironen, M. (1989). The Tampere schist belt: Structural style within an early Proterozoic volcanic arc system in southern Finland. *Precambrian Research*, *43*, 23–40. https://doi.org/10.1016/0301-9268(89)90003-X

Nironen, M. (1997). The Svecofennian Orogen: A tectonic model. *Precambrian Research*, *86*(1), 21–44. https://doi.org/10.1016/S0301-9268(97)00039-9

Nironen, M. (2003). Central Finland Granitoid Complex—Explanation to a map. *Geological Survey of Finland, Report of Investigation*, 157, 45 pp., Espoo.

Nironen, M. (2017). Guide to the geological map of Finland—Bedrock 1:1 000 000. In M. Nironen (Ed.), *Bedrock of Finland at the scale 1:1 000 000—Major stratigraphic units, metamorphism and tectonic evolution*, *Geological Survey of Finland, Special Paper* (Vol. 60, pp. 41–76). Espoo, Finland: Geological Survey of Finland.

Nironen, M., Elliott, B. A., & Rämö, O. T. (2000). 1.88–1.87 Ga post-kinematic intrusions of the Central Finland Granitoid Complex: A shift from C-type to A-type magmatism during lithospheric convergence. *Lithos*, *53*(1), 37–58. https://doi.org/10.1016/S0024-4937(00)00007-4

Nironen, M., Lahtinen, R., & Koistinen, T. (2002). Suomen geologiset aluenimet – yhtenäi sem pään nimikäytäntöön! Summary: Subdivision of Finnish bedrock—An attempt to harmonize terminology. *Geologi*, *54*(1), 8–14.

Pirttijärvi, M., Zaher, M. A., & Korja, T. (2014). Combined inversion of airborne electromagnetic and static magnetic field data. *Geophysica*, *50*(2), 65–87.

Rämö, O. T., Vaasjoki, M., Mättäri, I., Elliott, B. A., & Nironen, M. (2001). Petrogenesis of the post-kinematic magmatism of the Central Finland Granitoid Complex I; radiogenic isotope constraints and implications for crustal evolution. *Journal of Petrology*, *42*(11), 1971–1993. https://doi.org/10.1093/petrology/42.11.1971

Rao, C. K., Jones, A. G., & Moorkamp, M. (2007). The geometry of the Iapetus Suture Zone in central Ireland deduced from a magneto-telluric study. *Physics of the Earth and Planetary Interiors*, *161*(1), 134–141. https://doi.org/10.1016/j.pepi.2007.01.008

Rey, P. F., Teyssier, C., Kruckenberg, S. C., & Whitney, D. L. (2011). Viscous collision in channel explains double domes in metamorphic core complexes. *Geology*, *39*(4), 387–390. https://doi.org/10.1130/G31587.1

Rogers, J. J. W., & Santosh, M. (2002). Configuration of Columbia, a Mesoproterozoic supercontinent. *Gondwana Research*, *5*(1), 5–22. https://doi.org/10.1016/S1342-937X(05)70883-2

Rutland, R. W. R., Skiöld, T., & Page, R. W. (2001). Age of deformation episodes in the Palaeoproterozoic domain of northern Sweden, and evidence for a pre-1.9 Ga crustal layer. *Precambrian Research*, *112*(3), 239–259. https://doi.org/10.1016/S0301-9268(01)00166-8

Schulz, K. J., & Cannon, W. F. (2007). The Penokean orogeny in the Lake Superior region. *Precambrian Research*, *157*(1), 4–25. https://doi.org/10.1016/j.precamres.2007.02.022

Siivola, J., & Schmid, R. (2007). Recommendations by the IUGS Subcommission on the Systematics of Metamorphic Rocks: List of mineral abbreviations. *IUGS Commission on the Systematics in Petrology*, Web version 01.02.07. http://www.bgs.ac.uk/scmr/docs/papers/paper_12.pdf

Sipilä, P., Kujala, H., & Torssonen, M. (2008). Pre-Quaternary rocks of the Oravainen–Lapua–Alahärmä area, 40 pp., Geological Survey of Finland, Report of Investigation, 170.

Siripunvaraporn, W., & Egbert, G. (2000). An efficient data-subspace inversion method for 2-D magnetotelluric data. *Geophysics*, *65*(3), 791–803. https://doi.org/10.1190/1.1444778

Skiöld, T., & Rutland, R. W. R. (2006). Successive ~1.94Ga plutonism and ~1.92Ga deformation and metamorphism south of the Skellefte district, northern Sweden: Substantiation of the marginal basin accretion hypothesis of Svecofennian evolution. *Precambrian Research*, *148*(3), 181–204. https://doi.org/10.1016/j.precamres.2006.04.002

Smirnov, M. Y., & Pedersen, L. B. (2009). Magnetotelluric measurements across the Sorgenfrei-Tornquist Zone in southern Sweden and Denmark. *Geophysical Journal International*, *176*(2), 443–456. https://doi.org/10.1111/j.1365-246X.2008.03987.x

Sorjonen-Ward, P. (2006). Geological and structural framework and preliminary interpretation of the FIRE 3 and FIRE 3A reflection seismic profiles. In I. Kukkonen & R. Lahtinen (Eds.), *Finnish Reflection Experiment 2001–2005*, *Special Paper* (Vol. 43, pp. 105–159). Espoo: Geological Survey of Finland.

Suikkanen, E., Huhma, H., Kurhila, M., & Lahaye, Y. (2014). The age and origin of the Vaasa migmatite complex revisited. *Bulletin of the Geological Society of Finland*, *86*(1–2), 41–55.

Torvela, T., Moreau, J., Butler, R. W. H., Korja, A., & Heikkinen, P. (2013). The mode of deformation in the orogenic mid-crust revealed by seismic attribute analysis. *Geochemistry, Geophysics, Geosystems*, *14*(4), 1069–1086. https://doi.org/10.1002/ggge.20050

Vaarma, M., & Kähkönen, Y. (1994). Geochemistry of the Paleoproterozoic metavolcanic rocks at Evijärvi, western Finland. *Geological Survey of Finland Special Paper*, *19*, 47–59.

Vaarma, M., & Pipping, F. (1997). *Pre-Quaternary rocks of the Alajärvi and Evijärvi map-sheet areas. Sheets 2313 and 2314* (p. 83). Espoo: Geological Survey of Finland.

Vaittinen, K., Korja, T., Abdel Zaher, M., Pirttijärvi, M., Smirnov, M., Lahti, I., & Kaikkonen, P. (2012). Vintage and retro conductivity models of the Bothnian Bay region: implications for the crustal structure and processes of the Svecofennian orogen. In I. Kukkonen, E. Kosonen, K. Oinonen, O. Eklund, A. Korja, T. Korja, R. Lahtinen, J. P. Lunkka, & M. Poutanen (Eds.), *LITHOSPHERE 2012, Seventh Symposium on the Structure, Composition and Evolution of the Lithosphere in Finland Programme and extended abstracts, Report S-56* (pp. 105–108). Espoo: Institute of Seismology, University of Helsinki.

Vanderhaeghe, O. (2009). Migmatites, granites and orogeny: Flow modes of partially-molten rocks and magmas associated with melt/solid segregation in orogenic belts. *Tectonophysics*, *477*(3–4), 119–134. https://doi.org/10.1016/j.tecto.2009.06.021

Vanderhaeghe, O., Kruckenberg, S. C., Gerbault, M., Martin, L., Duchêne, S., & Deloule, E. (2018). Crustal-scale convection and diapiric upwelling of partially molten orogenic root (Naxos dome, Greece). *Tectonophysics*, *746*, 459–469. https://doi.org/10.1016/j.tecto.2018.03.007

Vanderhaeghe, O., & Teyssier, C. (2001). Partial melting and flow of orogens. *Tectonophysics*, *342*, 451–472. https://doi.org/10.1016/S0040-1951(01)00175-5

Ward, P. (1987). Early proterozoic deposition and deformation at the Karelian craton margin in southeastern Finland. *Precambrian Research*, *35*, 71–93. https://doi.org/10.1016/0301-9268(87)90046-5

Weil, A., Pastor-Galán, D., Johnston, S. T., & Gutiérrez-Alonso, G. (2019). Late/Post Variscan orocline formation and widespread magmatism. In C. Quesada & J. Oliveira (Eds.), *The geology of Iberia: A geodynamic approach*, *Regional Geology Reviews* (pp. 527–542). Cham: Springer. https://doi.org/10.1007/978-3-030-10519-8_14

Williams, I. S., Rutland, R. W. R., & Kousa, J. (2008). A regional 1.92Ga tectonothermal episode in Ostrobothnia, Finland: Implications for models of Svecofennian accretion. *Precambrian Research*, *165*(1), 15–36. https://doi.org/10.1016/j.precamres.2008.05.004

Williams, M. L., & Karlstrom, K. E. (1996). Looping P-T paths and high-T, low-P middle crustal metamorphism: Proterozoic evolution of the southwestern United States. *Geology*, *24*(12), 1119–1122. https://doi.org/10.1130/0091-7613(1996)024<1119:LPTPAH>2.3.CO;2

Zhao, G., Cawood, P. A., Wilde, S. A., & Sun, M. (2002). Review of global 2.1–1.8 Ga orogens: Implications for a pre-Rodinia supercontinent. *Earth-Science Reviews*, *59*(1), 125–162. https://doi.org/10.1016/S0012-8252(02)00073-9

Zhao, G., Sun, M., Wilde, S. A., & Li, S. (2004). A Paleo-Mesoproterozoic supercontinent: Assembly, growth and breakup. *Earth-Science Reviews*, *67*(1), 91–123. https://doi.org/10.1016/j.earscirev.2004.02.003